"Anti-p p interactions in the region x_T~1:the questions and the solutions at PANDA"

S.S. Shimanskiy (JINR, Dubna)

Plan

1. Counting rules for $\bar{p}p$

2. p_T~2 GeV/c anomaly, DINR and …

In 1973 were published two artiles :

Matveev V.A., Muradyan R.M., Tavkhelidze A.N. Lett. Nuovo Cimento 7,719 (1973);

Brodsky S., Farrar G. Phys. Rev. Lett. 31,1153 (1973)

Predictions that for momentum $p_{beam} \geq 5$ GeV/c in any binary large-angle scattering ($\theta_{cm} > 40^o$) reaction at large momentum transfers $Q = \sqrt{-t}$:

$$A + B \to C + D$$

$$\frac{d\sigma}{dt}_{A+B\to C+D} \sim s^{-(n_A+n_B+n_C+n_D-2)} f(\frac{t}{s})$$

where n_A, n_B, n_C and n_D the amounts of elementary constituents in A,B,C and D.

$s=(p_A+p_B)^2$ and $t=(p_A-p_C)^2$,

$$\frac{d\sigma}{dt}_{pp\to pp} \sim s^{-10} \quad \text{and} \quad \frac{d\sigma}{dt}_{\pi p\to \pi p} \sim s^{-8}$$

$a + b \Rightarrow c + d$

S. J. Brodsky and G. R. Farrar, Phys. Rev. Lett. **31**, 1153 (1973).

$$\frac{d\sigma}{dt}(a+b \Rightarrow c+d) = \frac{f(t/s)}{s^{n-2}}$$

$s \to \infty$

t/s *fixed*

$p + p \Rightarrow p + p \qquad s^{10}$

$\bar{p} + p \Rightarrow \bar{p} + p \qquad s^{10}$

$\bar{p} + d \Rightarrow \bar{p} + d \qquad s^{16}$

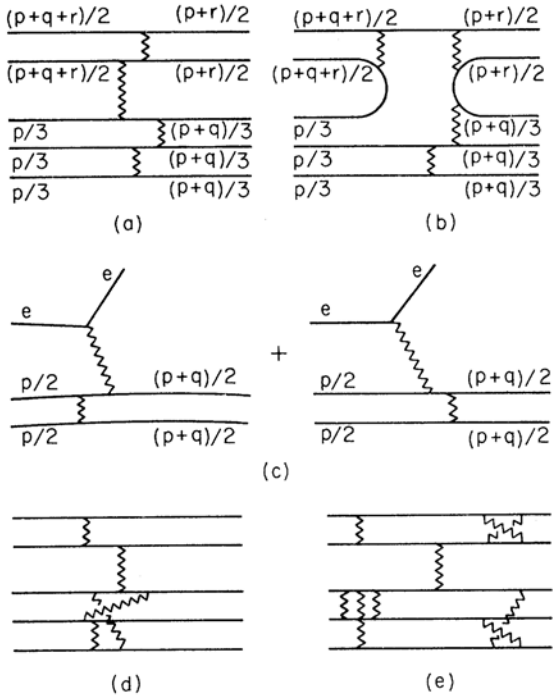

FIG. 1. Typical Born diagrams for large-momentum-transfer elastic scattering in the quark picture. (a) $\pi p \to \pi p$ (quark scattering), (b) $\pi p \to \pi p$ (quark interchange), (c) $e\pi \to e\pi$, (d) an irreducible loop diagram, (e) a reducible loop diagram.

SLAC – PUB – 4749
October 1988
(M)

ANTIPROTON ANNIHILATION IN QUANTUM CHROMODYNAMICS*

STANLEY J. BRODSKY

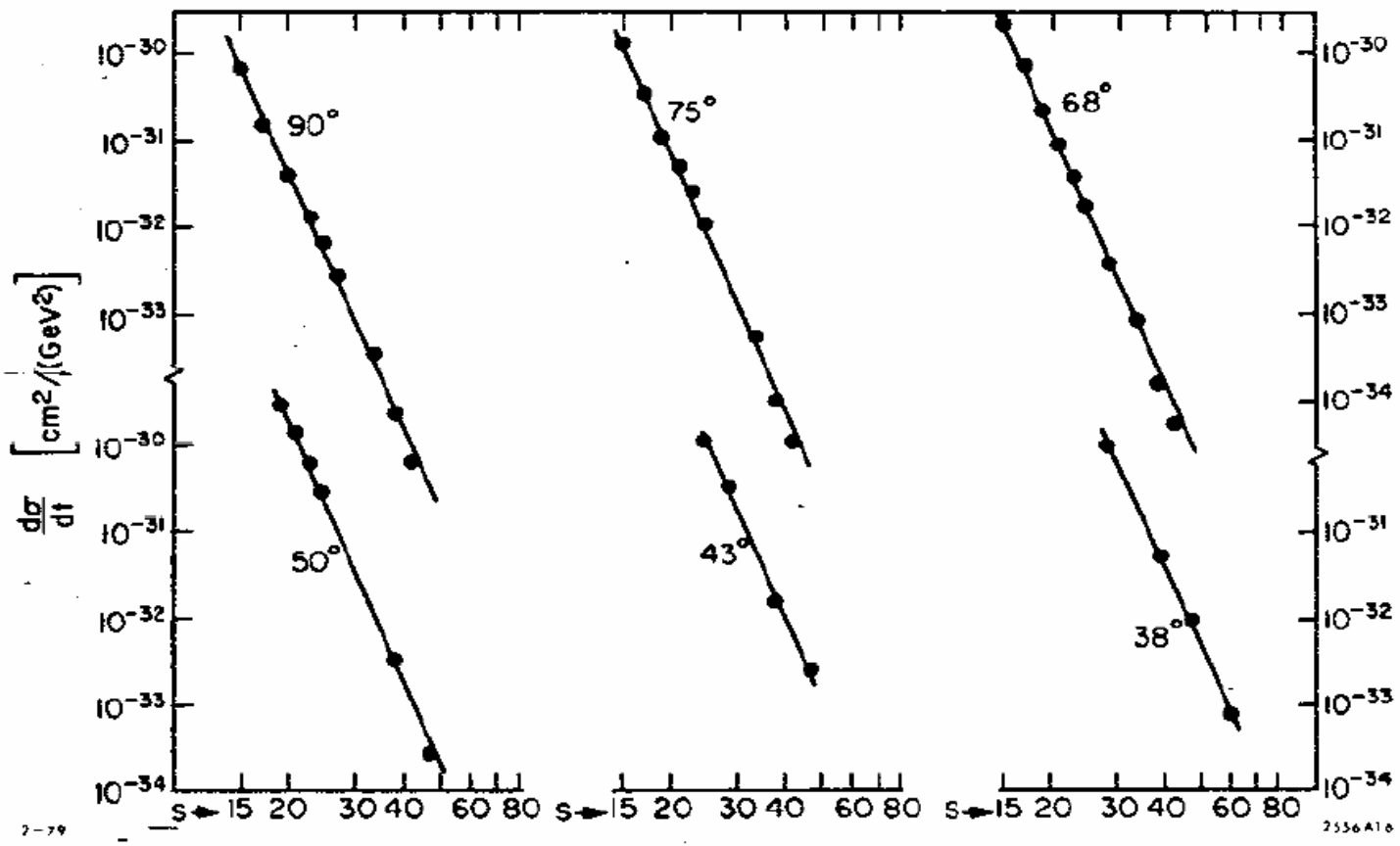

Fig. 16. Test of fixed θ_{CM} scaling for elastic pp scattering. The best fit gives the power $N = 9.7 \pm 0.5$ compared to the dimensional counting prediction N=10. Small deviations are not readily apparent on this log-log plot. The compilation is from Landshoff and Polkinghorne.

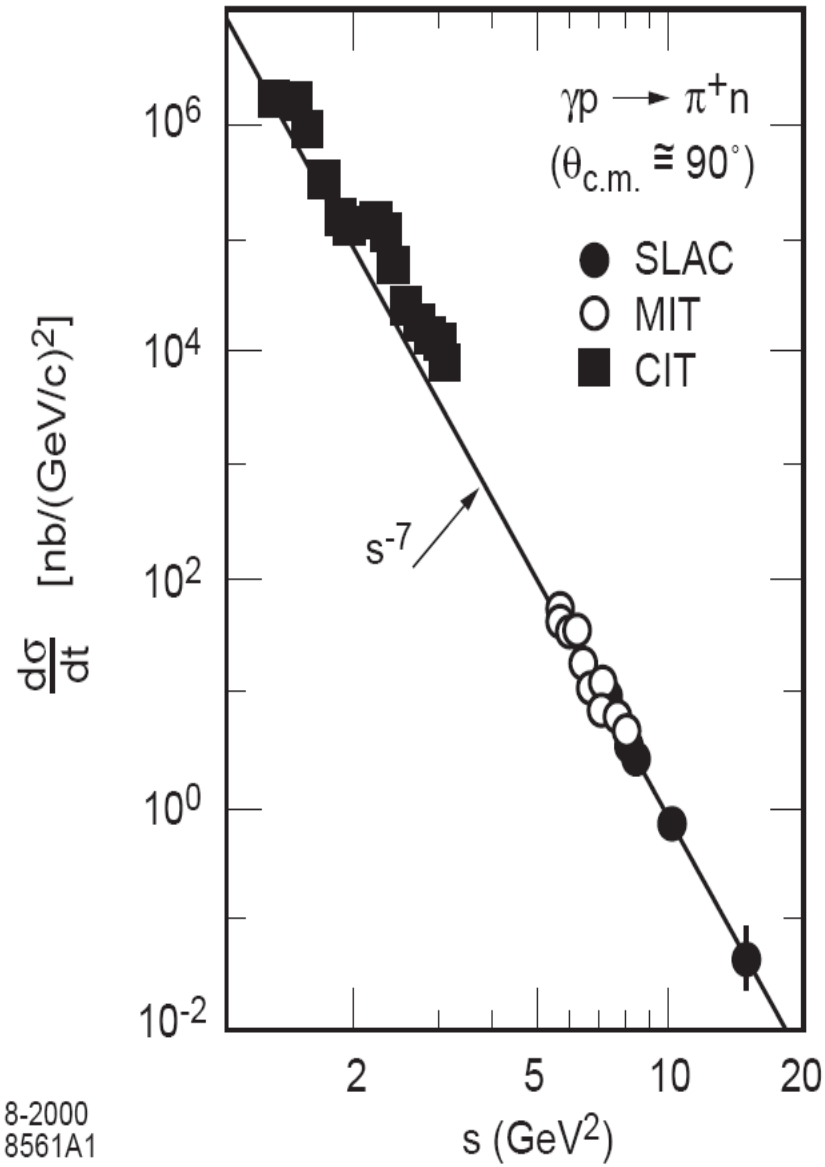
$\gamma p \rightarrow \pi^+ n$
$(\theta_{c.m.} \cong 90^\circ)$
SLAC
MIT
CIT
s^{-7}
$\frac{d\sigma}{dt}$ [nb/(GeV/c)^2]
10^6
10^4
10^2
10^0
10^{-2}
2
5
10
20
s (GeV^2)
8-2000
8561A1

Asymptotic form factors of hadrons and nuclei and the continuity of particle and nuclear dynamics

Stanley J. Brodsky*
Stanford Linear Accelerator Center, Stanford University, Stanford, California 94305

Benson T. Chertok†
American University, Washington, D. C. 20016

(Received 7 June 1976)

The large-q^2 behavior of the elastic form factor of a hadron or nucleus is related by dimensional counting to the number of its elementary constituents. Using the framework of a scale-invariant quark model, dimensional-scaling predictions are derived for the $B(q^2)/A(q^2)$ ratio in the Rosenbluth formula, multiple-photon-exchange corrections, and the mass parameters which control the onset of the asymptotic power law in the meson, nucleon, and deuteron form factors. A simple "democratic chain" model predicts that for large q^2, $F(q^2) \propto (1 - q^2/m_n^{\,2})^{1-n}$, where $m_n^{\,2}$ is proportional to the number of constituents n. In the case of nuclear targets (or systems with several scales of compositeness), we also define the "reduced" form factor $f_A(q^2) = F_A(q^2)/\Pi_{i=1}^{A} F_i(q_i^{\,2})$ in order to remove the minimal falloff of F_A due to the nucleon form factors at $q_i^{\,2} = (m_i^{\,2}/M_A^{\,2})q^2$. Dimensional counting predicts $(q^2)^{A-1} f_A(q^2) \to$ const. A systematic comparison of the data for π, p, n, and deuteron form factors with the dimensional-scaling quark-model predictions is given. Predictions are made for the large-spacelike-q^2 ^{3}He and α-particle form factors. We also relate the deuteron form factor to (off-shell) fixed-angle n-p scattering, and show that the experimental results for $t^5 F_d(t)$ are consistent with the magnitude of the s-wave wave function $u'(0)$ obtained from soft-core potentials. The relation of the dynamics of an underlying six-quark state of the deuteron to the nucleon-potential and meson-exchange-current contributions is discussed. The scaling of $q^2 f_d(q^2)$ implies that the nuclear potential (after removing the effects of nucleon structure) displays the scale-invariant behavior of a theory without a fundamental length scale. Predictions are also given for the structure functions, fragmentation, and large-angle scattering of a nucleus.

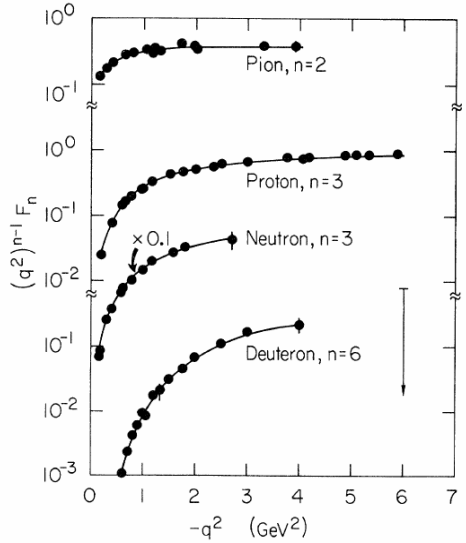

FIG. 1. Elastic electromagnetic form factors of hadrons for large spacelike q^2 in terms of the dimensional-scaling quark model. The curves simply connect the data points. (The neutron data have been multiplied by 0.1.)

$\gamma D \rightarrow p + n$

Phys.Rev. C70, 014005 (2004)

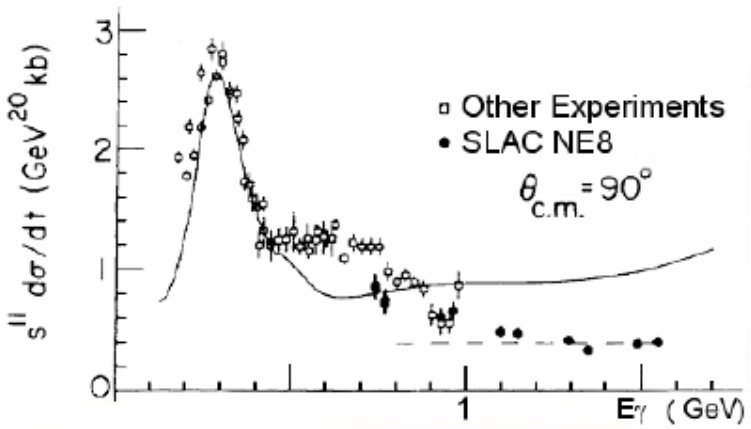

Figure 1.4: Results form the NE8 experiment: the cross section shows scaling for i photon energies larger then 1 GeV. The solid line represents a meson-nucleon desc which do not account for the data starting from 0.5 GeV of incident photon energy.

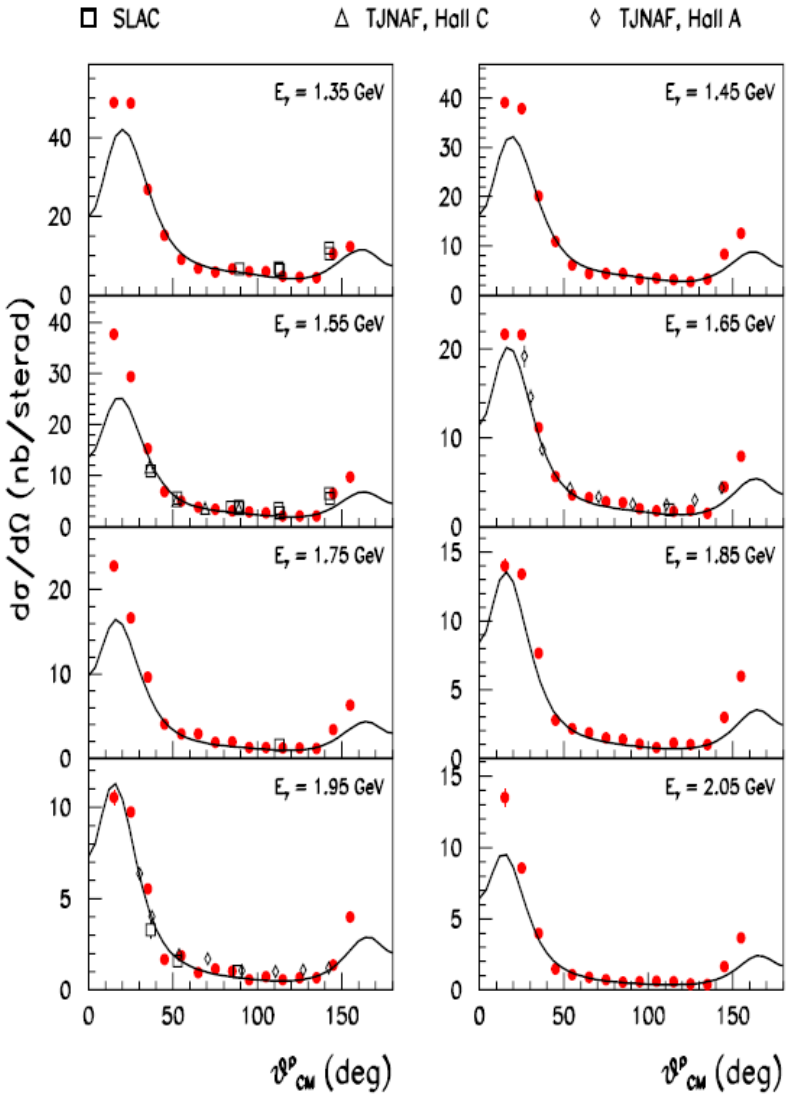

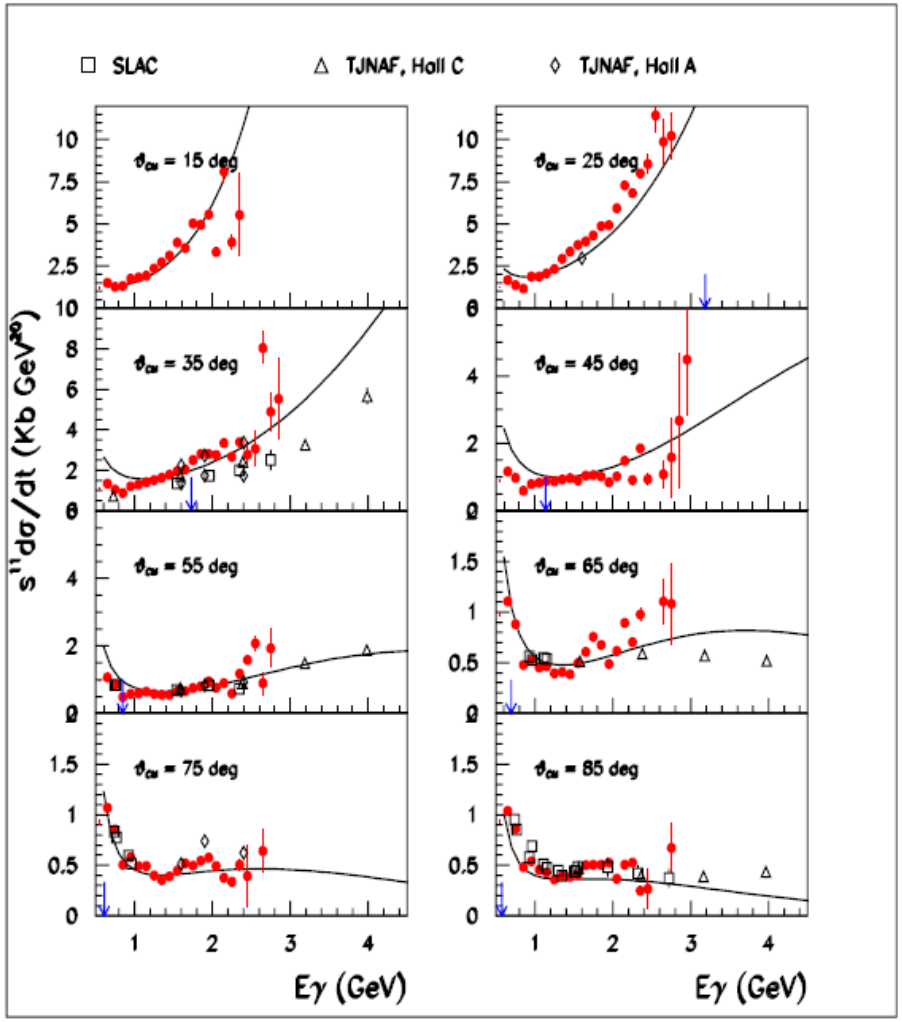
SLAC
TJNAF, Hall C
TJNAF, Hall A
θCM = 15 deg
θCM = 25 deg
θCM = 35 deg
θCM = 45 deg
θCM = 55 deg
θCM = 65 deg
θCM = 75 deg
θCM = 85 deg
s^11 dσ/dt (Kb GeV^20)
Eγ (GeV)

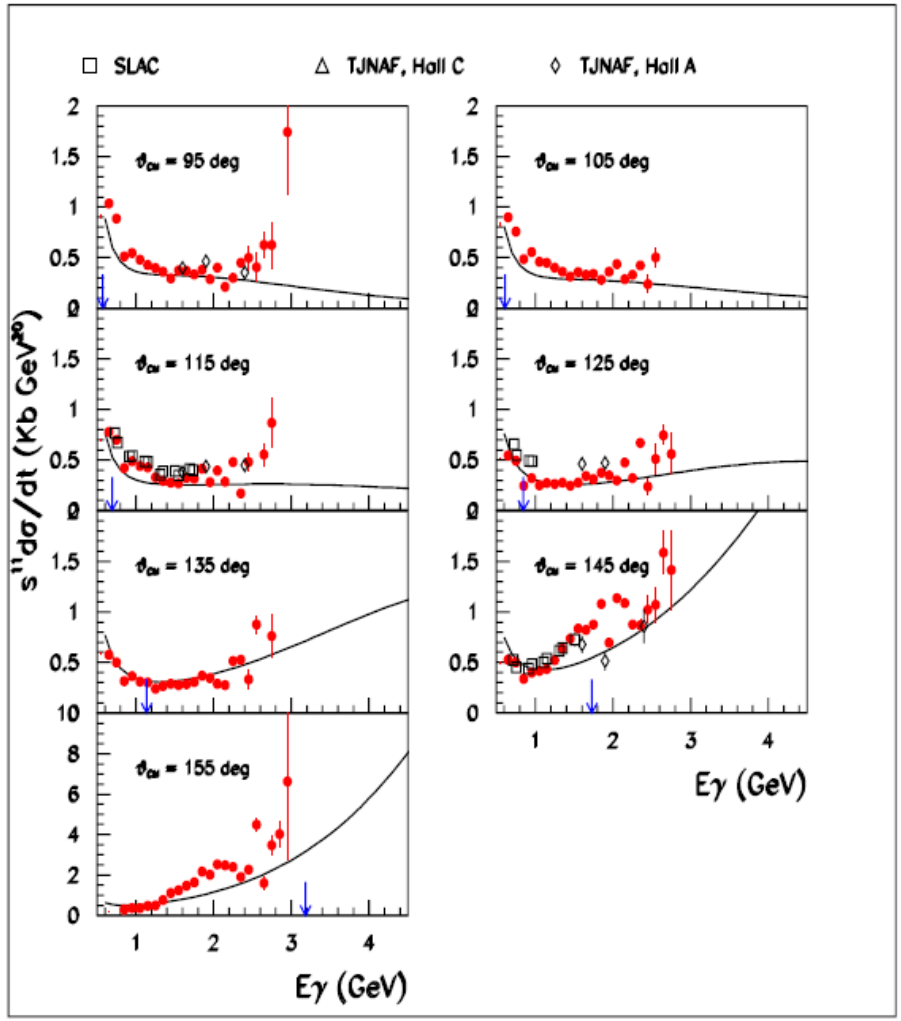
SLAC
TJNAF, Hall C
TJNAF, Hall A
θCM = 95 deg
θCM = 105 deg
θCM = 115 deg
θCM = 125 deg
θCM = 135 deg
θCM = 145 deg
θCM = 155 deg
s^11 dσ/dt (Kb GeV^20)
Eγ (GeV)

Light-Front QCD*

Stanley J. Brodsky

SLAC–PUB–10871
November 2004

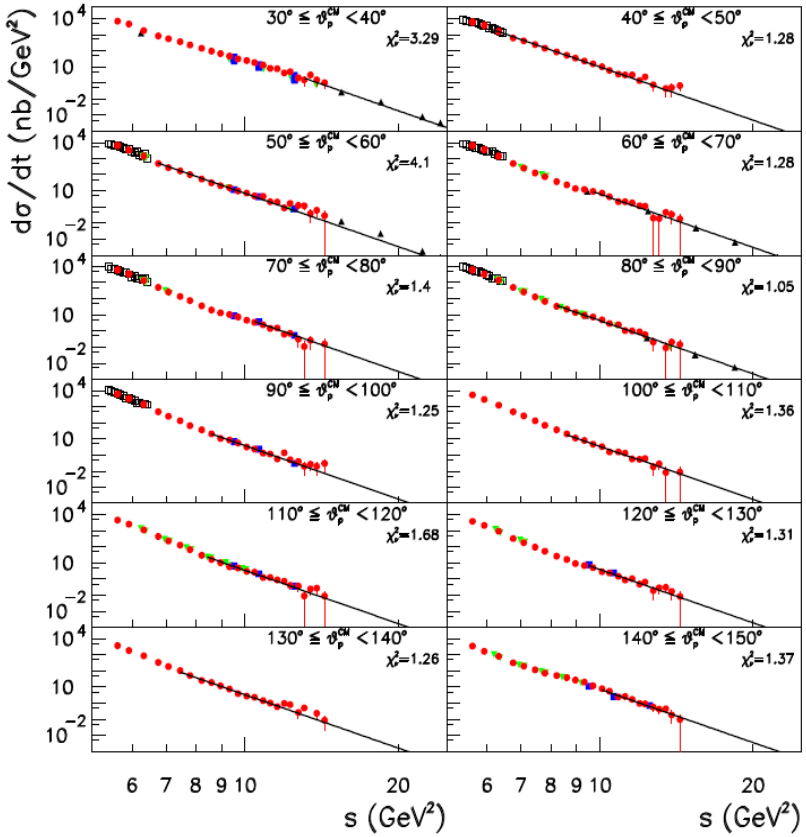

$$s^{11}\frac{d\sigma}{dt}(\gamma d \to pn) \sim$$

constant at fixed CM angle

Figure 8: Fits of the cross sections $d\sigma/dt$ to s^{-11} for $P_T \geq P_T^{th}$ and proton angles between 30° and 150° (solid lines). Data are from CLAS (full/red circles), Mainz(open/black squares), SLAC (full-down/green triangles), JLab Hall A (full/blue squares) and Hall C (full-up/black triangles). Also shown in each panel is the χ^2_ν value of the fit. From Ref. [160].

Pis'ma v ZhETF, vol. 81, iss. 7, pp. 387 – 390 © 2005 April 10

Indication of asymptotic scaling in the reactions $dd \to p^3\mathrm{H}$, $dd \to n^3\mathrm{He}$ and $pd \to pd$

Yu. N. Uzikov[1)]

Joint Institute for Nuclear Research, LNP, 141980 Dubna, Moscow region, Russia

Submitted 11 January 2005

Resubmitted 28 February 2005

It is shown that the differential cross sections of the reactions $dd \to n^3\mathrm{He}$ and $dd \to p^3\mathrm{H}$ measured at c.m.s. scattering angle $\theta_{cm} = 60^\circ$ in the interval of the deuteron beam energy 0.5–1.2 GeV demonstrate the scaling behaviour, $d\sigma/dt \sim s^{-22}$, which follows from constituent quark counting rules. It is found also that the differential cross section of the elastic $dp \to dp$ scattering at $\theta_{cm} = 125-135^\circ$ follows the scaling regime $\sim s^{-16}$ at beam energies 0.5–5 GeV. These data are parameterized here using the Reggeon exchange.

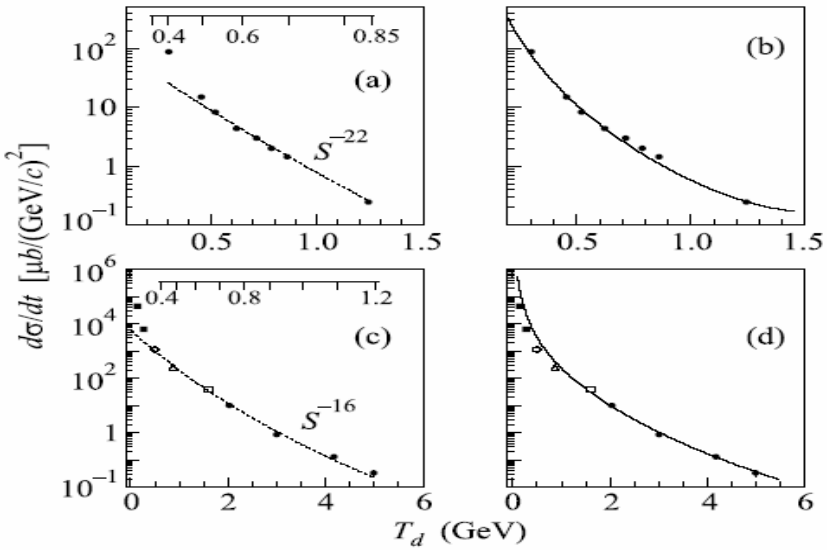

Fig.2. The differential cross section of the $dd \to n^3\mathrm{He}$ and $dd \to p^3\mathrm{H}$ reactions at $\theta_{cm} = 60^o$ (a), (b) and $dp \to dp$ at $\theta_{cm} = 127^o$ (c), (d) versus the deuteron beam kinetic energy. Experimental data in (a), (b) are taken from [20]. In (c), (d), the experimental data (black squares),(○), (△), (open square) and (●) are taken from [22 – 26], respectively. The dashed curves give the s^{-22} (a) and s^{-16} (c) behaviour. The full curves show the result of calculations using Regge formalism given by Eqs. (2), (3), (4) with the following parameters: (b) – $C_1 = 1.9\,\mathrm{GeV}^2$, $R_1^2 = 0.2\,\mathrm{GeV}^{-2}$, $C_2 = 3.5$, $R_2^2 = -0.1\,\mathrm{GeV}^{-2}$; (d) – $C_1 = 7.2\,\mathrm{GeV}^2$, $R_1^2 = 0.5\,\mathrm{GeV}^{-2}$, $C_2 = 1.8$, $R_2^2 = -0.1\,\mathrm{GeV}^{-2}$. The upper scales in (a) and (c) show the relative momentum q_{pn} (GeV/c) in the deuteron for the ONE mechanism

Unified description of inclusive and exclusive reactions at all momentum transfers*

R. Blankenbecler and S. J. Brodsky

$$E\frac{d\sigma}{d^3p}(A+B\to C+X)\to(p_T^2)^{-N}f\left(\frac{\mathfrak{M}^2}{s},\frac{t}{s}\right)$$

and[5,6]

$$\frac{d\sigma}{dt}(A+B\to C+D)\to(p_T^2)^{-N}f\left(\frac{t}{s}\right)$$

The entire kinematic range of high-energy inclusive reactions is illustrated on the Peyrou plot of Fig. 1. As usual we define

$$s=(p_A+p_B)^2,\quad t=(p_A-p_C)^2,$$

$$u=(p_B-p_C)^2,\quad \mathfrak{M}^2=(p_A+p_B-p_C)^2,$$

and

$$\epsilon=\mathfrak{M}^2/s\cong(1-p_{\text{c.m.}}/p_{\max}),$$

$$x_T=p_T/p_{\max},\quad x_L=p_L/p_{\max}\simeq(t-u)/s.$$

TABLE I. The expected dominant subprocesses for selected hadronic inclusive reactions at large transverse momentum. The second column lists the important exclusive processes which contribute to each inclusive cross section at $\epsilon\sim 0$. The basic subprocesses expected in the CIM, and the resulting form of the inclusive cross section $Ed\sigma/d^3p\sim(p_\perp{}^2)^{-N}\epsilon^P$ for $p_\perp{}^2\sim\infty$, $\epsilon\to 0$, and fixed $\theta_{\text{c.m.}}$ are given in the last columns. The subprocesses that have the dominant $p_\perp$ dependence at fixed ϵ are underlined. For some particular final-state quantum numbers, the above powers of ϵ should be increased.

Inclusive process	Exclusive-limit channel	Subprocesses	$\frac{d\sigma}{d^3p/E}$ $(\theta\sim 90°)$
$M+B\to M+X$	$M+B\to M+B^*$ $(n=10)$	$\underline{M+q\to M+q}$	$(p_\perp{}^2)^{-4}\epsilon^3$
		$\underline{\bar q+B\to M+qq}$	$(p_\perp{}^2)^{-6}\epsilon^1$
		$M+B\to M+B^*$	$(p_\perp{}^2)^{-8}\epsilon^{-1}$
$B+B\to B+X$	$B+B\to B+B^*$ $(n=12)$	$\underline{B+q\to B+q}$	$(p_\perp{}^2)^{-6}\epsilon^3$
		$\underline{(qq)+(qq)\to B+q}$	$(p_\perp{}^2)^{-6}\epsilon^3$
		$\underline{B+(qq)\to B+qq}$	$(p_\perp{}^2)^{-8}\epsilon^1$
		$B+B\to B+B^*$	$(p_\perp{}^2)^{-10}\epsilon^{-1}$
	$B+B\to B+B^*+M^*$ $(n=14)$	$\underline{q+q\to B+\bar q}$	$(p_\perp{}^2)^{-4}\epsilon^7$
		$q+(qq)\to B+M^*$	$(p_\perp{}^2)^{-6}\epsilon^5$
		$(qq)+B\to B+M^*+qq$	$(p_\perp{}^2)^{-10}\epsilon^1$
		$B+B\to B+B^*+M^*$	$(p_\perp{}^2)^{-12}\epsilon^{-1}$
$B+B\to M+X$	$B+B\to M+B^*+B^*$ $(n=14)$	$\underline{q+(qq)\to M+B^*}$	$(p_\perp{}^2)^{-6}\epsilon^5$
		$q+B\to q(\to M+q)+B^*$	$(p_\perp{}^2)^{-6}\epsilon^5$
		$q+B\to M+q+B^*$	$(p_\perp{}^2)^{-8}\epsilon^3$
		$(qq)+B\to M+B^*+qq$	$(p_\perp{}^2)^{-10}\epsilon^1$
		$B+B\to M+B^*+B^*$	$(p_\perp{}^2)^{-12}\epsilon^{-1}$
	$B+B\to M+M^*+B^*+B^*$ $(n=16)$	$\underline{M+q\to M+q}$	$(p_\perp{}^2)^{-4}\epsilon^9$
		$q+q\to\bar q(\to M+\bar q)+B^*$	$(p_\perp{}^2)^{-4}\epsilon^9$
		$q+q\to M+B^*+\bar q$	$(p_\perp{}^2)^{-6}\epsilon^7$
		$M+B\to M+B^*$	$(p_\perp{}^2)^{-8}\epsilon^5$
	$B+B\to M+M^*+M^*+B^*+B^*$ $(n=18)$	$\underline{q+\bar q\to M+M^*}$	$(p_\perp{}^2)^{-4}\epsilon^{11}$
		$\underline{q+M\to q(\to M+q)+M^*}$	$(p_\perp{}^2)^{-4}\epsilon^{11}$
$B+B\to\bar B+X$	$B+B\to\bar B+B^*+B^*+\overline{B^*}$ $(n=18)$	$\underline{q+q\to B^*+\bar q(\to\bar B+qq)}$	$(p_\perp{}^2)^{-4}\epsilon^{11}$
		$q+q\to B^*+\bar B+qq$	$(p_\perp{}^2)^{-8}\epsilon^7$
		$q+(qq)\to\bar B+B^*+B^*$	$(p_\perp{}^2)^{-10}\epsilon^5$

S.J. Brodsky, J.F.Gunion

SLAC-PUB-1806
August 1976
(T/E)

RECENT DEVELOPMENTS IN THE THEORY OF LARGE TRANSVERSE MOMENTUM PROCESSES*

TABLE I

Scaling Predictions for $E\, d\sigma/d^3p = C\, p_T^{-n}(1-x_T)^F$

Large p_T Process	Leading CIM Subprocess	Predicted	Observed (CP)[3]
		n//F	n//F
$pp \to \pi^+ X$	$qM \to q\pi^+$	8//9	8.5//8.8
π^-	$qM \to q\pi^-$	8//9	8.9//9.7
K^+	$qM \to qK^+$	8//9	8.4//8.8
K^-	$qM \to qK^-$	8//13	8.9//11.7
	$q\bar{q} \to K^+K^-$	8//11	
$pp \to pX$	$q(qq) \to Mp$	12//5	11.7//6.8
	$qB \to qp$	12//7	
$pp \to \bar{p}X$	$q\bar{q} \to B\bar{p}$	12//11	8.8//14.2
	$qM \to qM$	8//15	
$\pi p \to \pi X$	$q\bar{q} \to M\pi$	8//5	
	$qM \to q\pi$	8//7	
	$q(qq) \to B\pi$	12//3	
	$\pi q \to \pi q$	8//3	

$\overline{p}p$ - data in the x_T~1 region

Data compilation

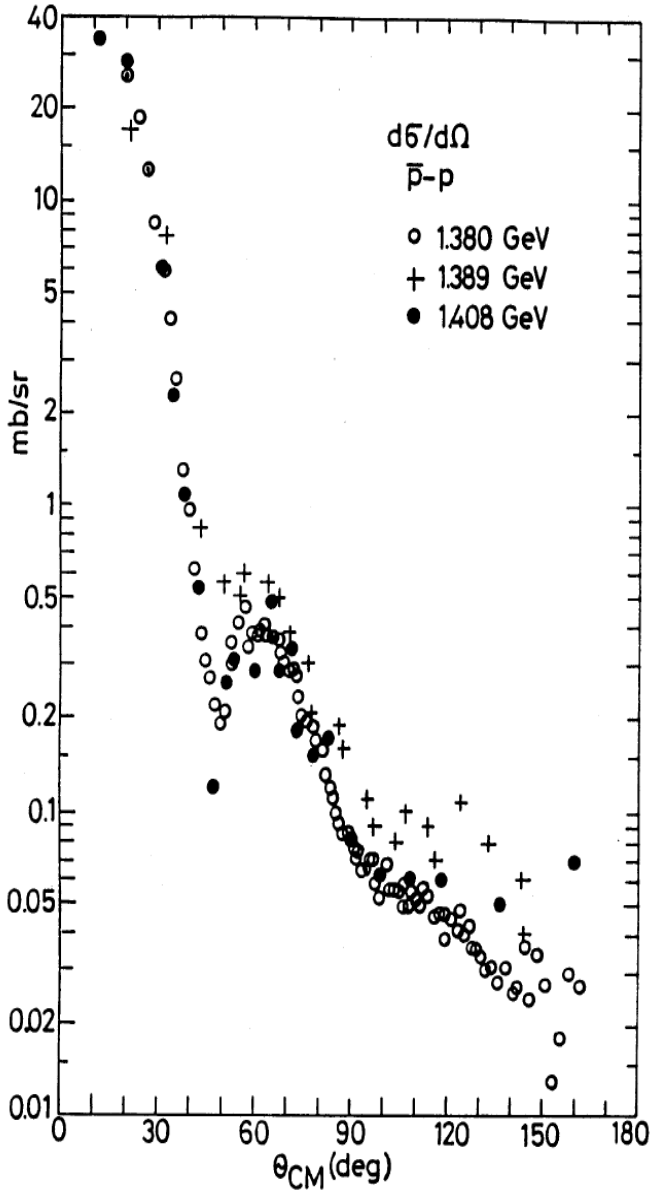

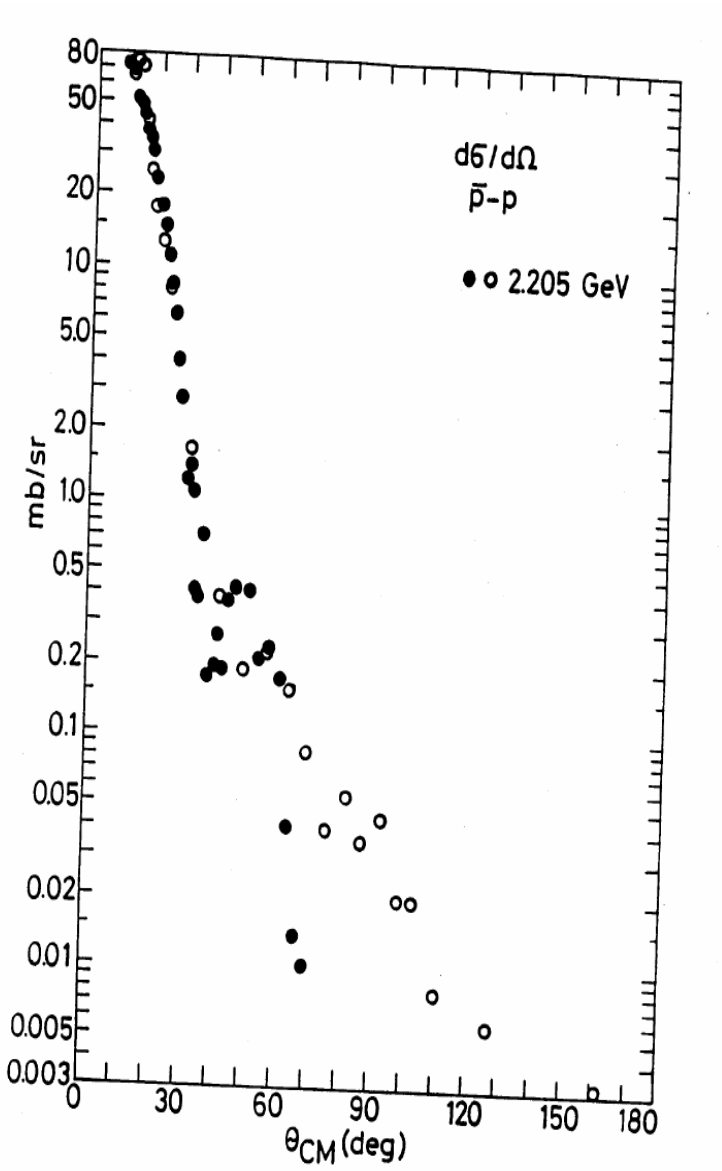

Nuclear Physics B97 (1975) 11–28

ANTIPROTON-PROTON ELASTIC SCATTERING AT 6.2 GeV/c

T. BURAN[1], A. EIDE[2,3], P. HELGAKER[1], P. LEHMANN, A. LUNDBY, A. NAVARRO-SAVOY, L. STAURSET[1] and O. SØRUM[1]
CERN, Geneva, Switzerland

Table 1
Summary of results for the measurements of the antiproton–proton elastic scattering cross section at 90° CM.

P [GeV/c]	N	L [nb^{-1}]	$d\sigma/d\Omega$ [μb/ster]	$-t$ [(GeV/c)^2]	$d\sigma/dt$ [μb/(GeV/c)^2]	Relative error(%)	
						stat	syst
3.65	3151	12.04	4.75	2.65	11.20	1.8	10.0
3.83	684	2.16	4.12	2.78	9.29	3.8	10.0
4.07	1577	10.32	2.23	3.03	4.61	2.6	10.0
5.65	107	21.06	0.043	4.50	0.060	19.0	13.0

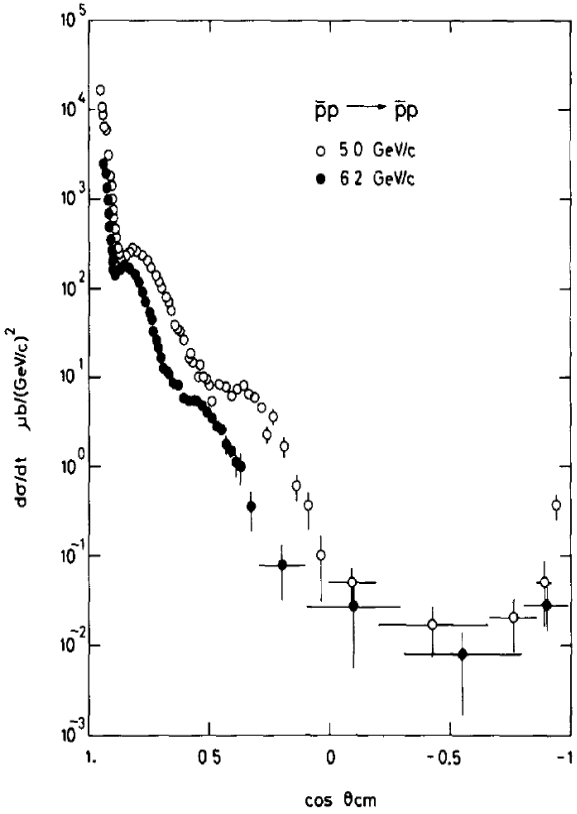

Fig 6 The differential cross section for $\bar{p}p$ elastic scattering as a function of $\cos\theta_{cm}$, for this experiment and our earlier experiment at 5 GeV/c (ref. [1]).

Comparison of 20 exclusive reactions at large t

C. White,[4,*] R. Appel,[1,5,†] D. S. Barton,[1] G. Bunce,[1] A. S. Carroll,[1]
H. Courant,[4] G. Fang,[4,‡] S. Gushue,[1] K. J. Heller,[4] S. Heppelmann,[2]
K. Johns,[4,§] M. Kmit,[1,‖] D. I. Lowenstein,[1] X. Ma,[3] Y. I. Makdisi,[1]
M. L. Marshak,[4] J. J. Russell,[3]
and M. Shupe[4,§]

TABLE IV. Cross sections at 90 degrees and 5.9 GeV/c incident beam momentum. Reaction number refers to Fig. 27. The values represent interpolations where the range spans 90°.

Number	Reaction	Cross section [nb/(GeV/c)^2]
1	$\pi^+ p \to p\pi^+$	132 ± 10
2	$\pi^- p \to p\pi^-$	73 ± 5
3	$K^+ p \to pK^+$	219 ± 30
4	$K^- p \to pK^-$	18 ± 6
5	$\pi^+ p \to p\rho^+$	214 ± 30
6	$\pi^- p \to p\rho^-$	99 ± 13
7	$K^+ p \to pK^{*+}$	$291 + 47 - 130$
8	$K^- p \to pK^{*-}$	$15 + 10 - 13$
9	$K^- p \to \pi^- \Sigma^+$	50 ± 21
10	$K^- p \to \pi^+ \Sigma^-$	4 ± 3
11	$K^- p \to \Lambda\pi^0$	< 80
12	$\pi^- p \to \Lambda K^0$	< 5
13	$\pi^+ p \to \pi^+ \Delta^+$	45 ± 10
14	$\pi^- p \to \pi^- \Delta^+$	20 ± 11
15	$\pi^- p \to \pi^+ \Delta^-$	24 ± 5
16	$K^+ p \to K^+ \Delta^+$	< 230
17	$pp \to pp$	3300 ± 40
18	$\bar{p}p \to p\bar{p}$	75 ± 8
19	$\bar{p}p \to \pi^+ \pi^-$	7 ± 3
20	$\bar{p}p \to K^+ K^-$	2 ± 2

TABLE V. The scaling between E755 and E838 has been measured for eight meson-baryon and 2 baryon-baryon interactions at $\theta_{\text{c.m.}} = 90°$. The nominal beam momentum was 5.9 GeV/c and 9.9 GeV/c for E838 and E755, respectively. There is also an overall systematic error of $\Delta n_{\text{syst}} = \pm 0.3$ from systematic errors of $\pm 13\%$ for E838 and $\pm 9\%$ for E755.

		Cross section		n-2
No.	Interaction	E838	E755	$(\frac{d\sigma}{dt} \sim 1/s^{n-2})$
1	$\pi^+ p \to p\pi^+$	132 ± 10	4.6 ± 0.3	6.7 ± 0.2
2	$\pi^- p \to p\pi^-$	73 ± 5	1.7 ± 0.2	7.5 ± 0.3
3	$K^+ p \to pK^+$	219 ± 30	3.4 ± 1.4	$8.3^{+0.6}_{-1.0}$
4	$K^- p \to pK^-$	18 ± 6	0.9 ± 0.9	≥ 3.9
5	$\pi^+ p \to p\rho^+$	214 ± 30	3.4 ± 0.7	8.3 ± 0.5
6	$\pi^- p \to p\rho^-$	99 ± 13	1.3 ± 0.6	8.7 ± 1.0
13	$\pi^+ p \to \pi^+ \Delta^+$	45 ± 10	2.0 ± 0.6	6.2 ± 0.8
15	$\pi^- p \to \pi^+ \Delta^-$	24 ± 5	< 0.12	> 10.1
17	$pp \to pp$	3300 ± 40	48 ± 5	9.1 ± 0.2
18	$\bar{p}p \to p\bar{p}$	75 ± 8	≤ 2.1	≥ 7.5

PRECISION MEASUREMENTS OF THE ANTIPROTON-PROTON ELASTIC SCATTERING CROSS SECTION AT 90° IN THE INCIDENT MOMENTUM RANGE BETWEEN 3.5 GeV/*c* AND 5.7 GeV/*c*

R-704 Collaboration

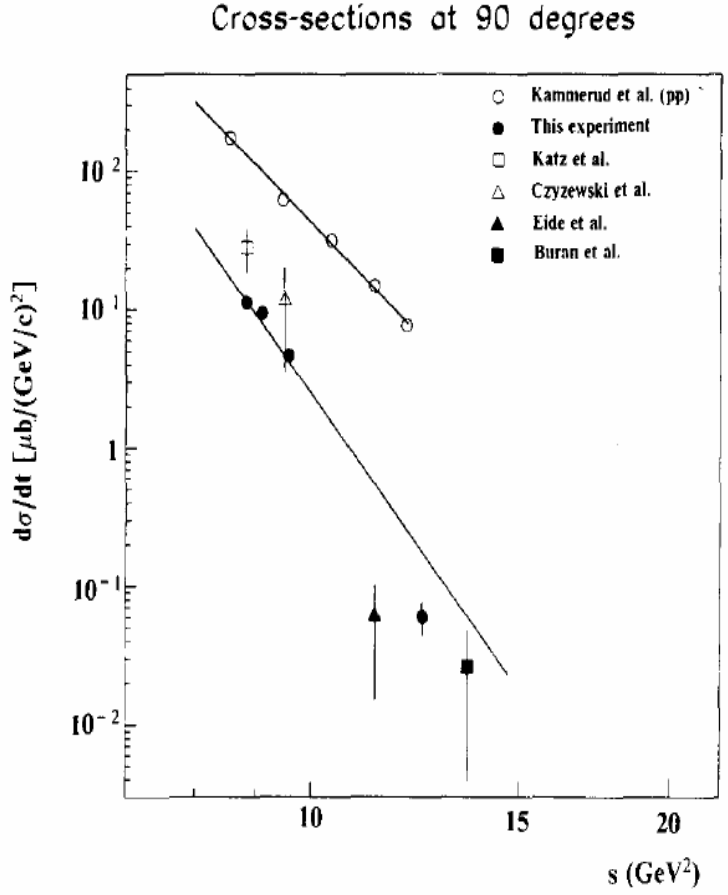

Fig. 3. The $p\bar{p}$ and pp elastic differential cross sections at 90° CM as function of the square of the CM energy, s. Open circles are pp data from ref. [6]. These data fit well to the drawn curve proportional to s^{-9}. The remaining points are $p\bar{p}$ data. Shaded from this experiment. Otherwise from ref. [7] (open square), ref. [8] (open triangle) ref. [9] (shaded triangle) and ref. [10] (shaded square). The lower curve is an s^{-n} fit to four data points of this experiment, neglecting systematic errors. One obtains $n = 12.3 \pm 0.2$, but evidently the data do not seem to follow this kind of a power law.

The challenge for PANDA

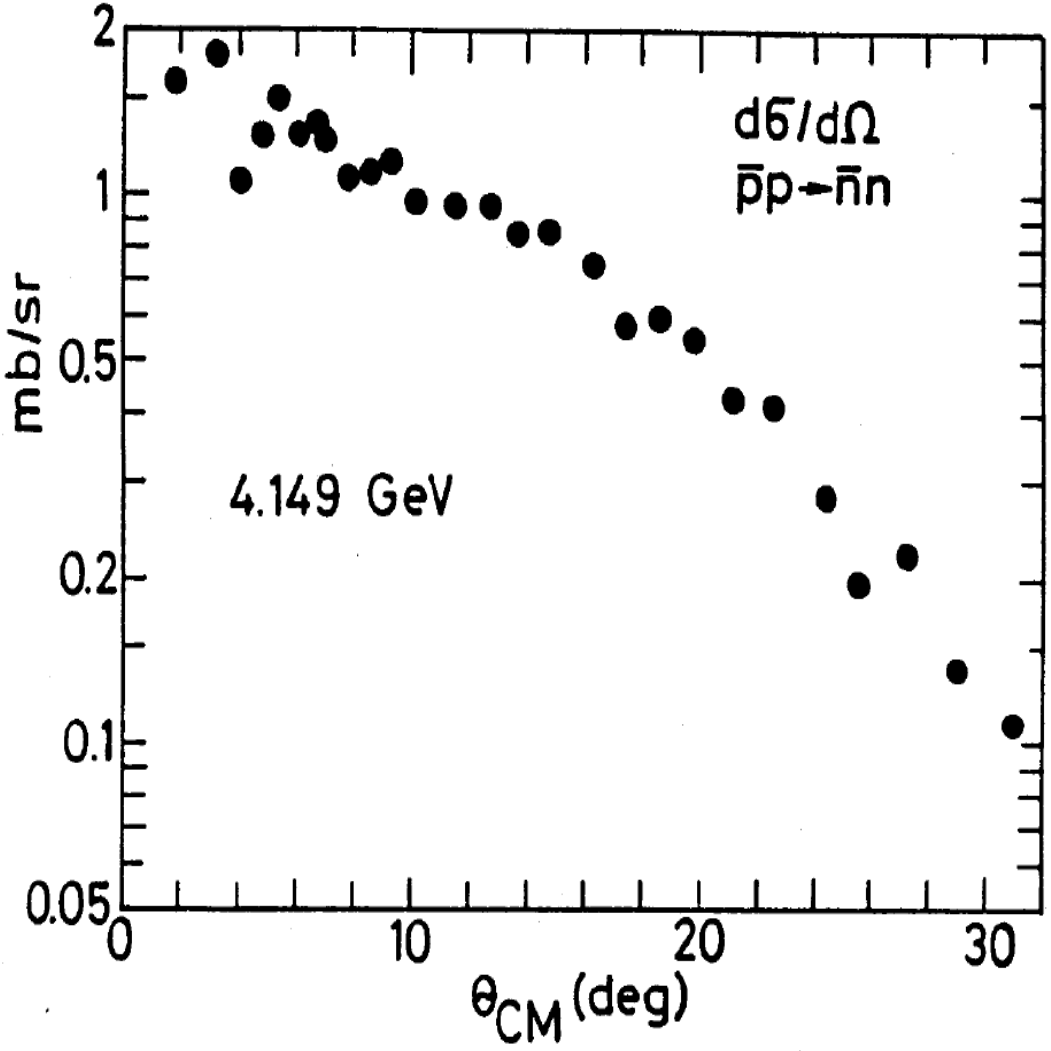

p_T~2 GeV/c anomaly

Spin Correlations, QCD Color Transparency, and Heavy-Quark Thresholds in Proton-Proton Scattering

Stanley J. Brodsky and Guy F. de Teramond
Stanford Linear Accelerator Center, Stanford University, Stanford, California 94305
(Received 14 January 1988)

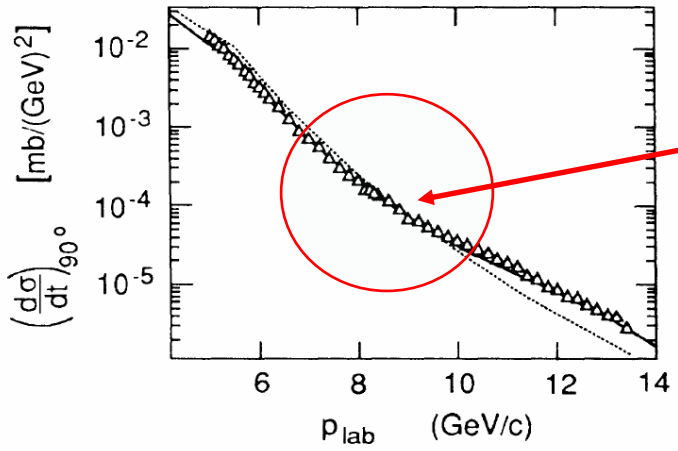

FIG. 1. Prediction (solid curve) for $d\sigma/dt$ compared with the data of Akerlof *et al.* (Ref. 16). The dotted line is the background PQCD prediction.

[16]K. Abe *et al.*, Phys. Rev. D **12**, 1 (1975), and references therein. The high-energy data for $d\sigma/dt$ at $\theta_{c.m.} = \pi/2$ are from C. W. Akerlof *et al.*, Phys. Rev. **159**, 1138 (1967); G. Cocconi *et al.*, Phys. Rev. Lett. **11**, 499 (1963); J. V. Allaby *et al.*, Phys. Lett. **23**, 389 (1966).

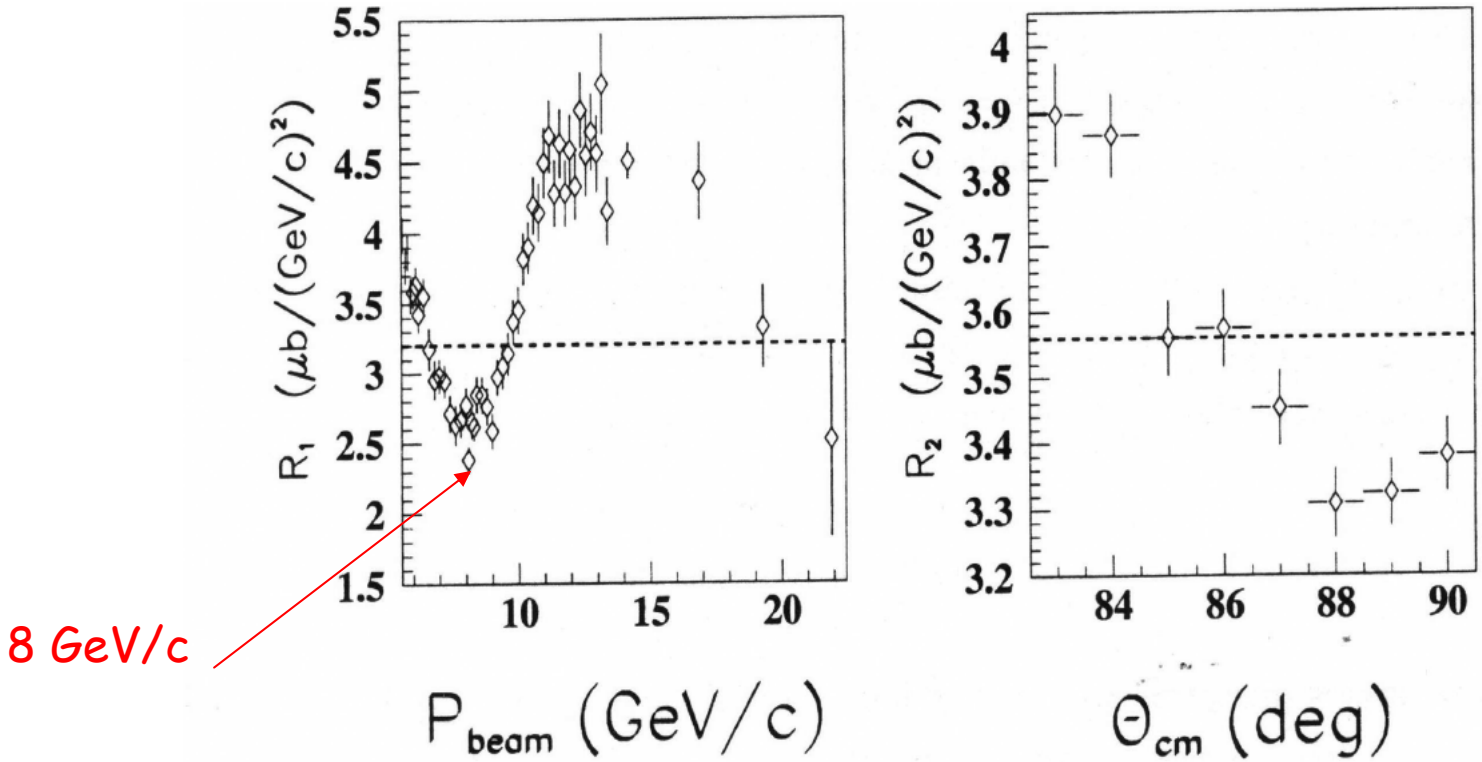

Figure 1.2: Scaled $pp \to pp$ differential cross sections. The dashed lines represent perfect scaling. Their vertical position is arbitrary. **Left** - $R_1 = ((\frac{s}{s_0})^{10} \frac{d\sigma}{dt}(pp))^{-1}$ $(s_0 = 13\ GeV^2)$ at $\theta_{cm} = 90^0$ versus incoming momentum. Data are from Ref. [19]. **Right** - $R_2 = (1 - \cos^2\theta_{cm})^{4\gamma} \frac{d\sigma}{dt}(pp)$ $(\gamma = 1.6)$ at $p_{lab} = 5.9$ GeV/c versus θ_{cm}. Data are from Ref. [17].

PHYSICAL REVIEW D VOLUME 23, NUMBER 3 1 FEBRUARY 1981

Energy dependence of spin-spin effects in p-p elastic scattering at 90°$_{c.m.}$

E. A. Crosbie, L. G. Ratner, and P. F. Schultz
Argonne National Laboratory, Argonne, Illinois 60439

J. R. O'Fallon
Argonne Universities Association, Argonne, Illinois 60439

D. G. Crabb, R. C. Fernow,* P. H. Hansen,† A. D. Krisch, A. J. Salthouse,‡ B. Sandler,§ T. Shima, and K. M. Terwilliger
Randall Laboratory of Physics, The University of Michigan, Ann Arbor, Michigan 48109

N. L. Karmakar
University of Kiel, Kiel, Germany

S. L. Linn‖ and A. Perlmutter
Department of Physics and Center for Theoretical Studies, The University of Miami, Coral Gables, Florida 33124

P. Kyberd
Nuclear Physics Laboratory, Oxford University, Oxford, England
(Received 31 March 1980)

The energy dependence of the spin-parallel and spin-antiparallel cross sections for $p_\uparrow + p_\uparrow \to p + p$ at 90°$_{c.m.}$ was measured for beam momenta between 6 and 12.75 GeV/c. The ratio $(d\sigma/dt)_{\text{parallel}}:(d\sigma/dt)_{\text{antiparallel}}$ at 90° is about 1.2 up to 8 GeV/c and then increases rapidly to a value of almost 4 near 11 GeV/c. Our data indicate that this ratio may depend only on the variable $P_\perp{}^2$, and suggests that the ratio may reach a limiting value of about 4 for large $P_\perp{}^2$.

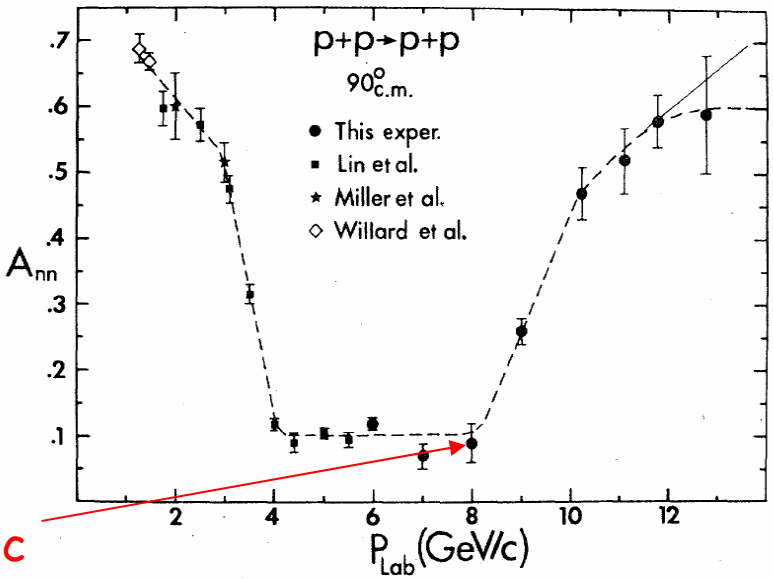

8 GeV/c

FIG. 2. Plot of the spin-spin correlation parameter A_{nn} for $p+p \to p+p$ at 90°$_{c.m.}$ as a function of incident beam momentum. The dashed and solid lines are hand-drawn possible fits.

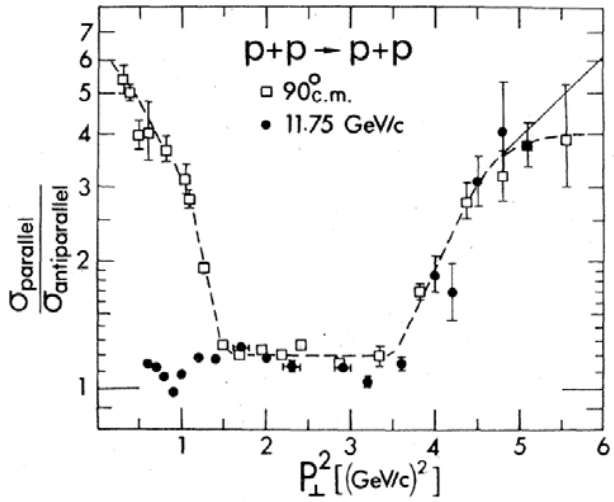

FIG. 3. Plot of the ratio of the spin-parallel to spin-antiparallel differential cross sections, as a function of $P_\perp{}^2$, for p-p elastic scattering. The squares are the fixed-angle data at 90°$_{c.m.}$, with the incident energy varied. The circles are data (Refs. 5, 11) with the momentum held fixed at 11.75 GeV/c while the scattering angle is varied. The dashed and solid lines are hand-drawn possible fits to the 90°$_{c.m.}$ data.

PRECISION MEASUREMENTS OF THE ANTIPROTON–PROTON ELASTIC SCATTERING CROSS SECTION AT 90° IN THE INCIDENT MOMENTUM RANGE BETWEEN 3.5 GeV/*c* AND 5.7 GeV/*c*

R-704 Collaboration

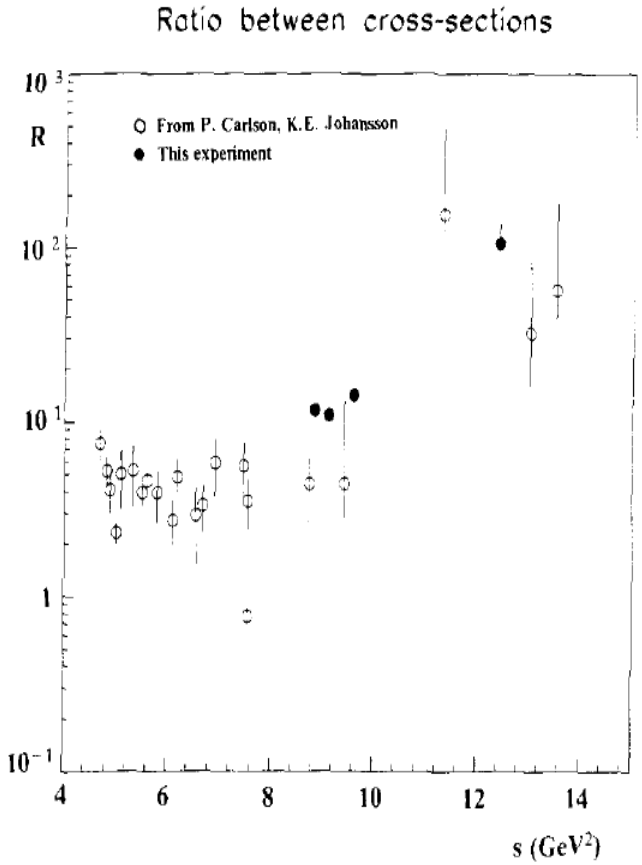

Fig. 4. The ratio between pp and $p\bar{p}$ elastic cross sections at 90° as function of s. The figure is taken from ref. [13] with our data points (shaded circles) added. The pp data used for calculating these ratios for our data points are from ref. [6].

E2-85-537

A.V.Efremov, V.T.Kim, G.I.Lykasov

HARD HADRON-NUCLEUS PROCESSES AND MULTIQUARK CONFIGURATIONS IN NUCLEI

V. Conclusion

The analysis of the inclusive large x_1 meson production in the hard hadron processes on nuclei has allowed one to understand the relative contribution of multiple rescattering processes and the existence of multiquark fluctons in the nucleus in dependence on x_1 the multiple rescattering processes are dominating at $x_1 < 0.7 \div 0.8$ whereas at larger x_1 the mechanism of hard scattering on fluctons is dominating. The model of multiple rescattering in which the multiple soft collisions suggested in this paper are taken into account before the hard collision allows one to describe the multiple rescattering processes inside the nucleus correctly.

The fluctons model succesfully used earlier for the description of the cumulative production and EMC-effect with such parameters is applied for the description of anomalous phenomena in the large p_1 processes in nuclei.

Exclusive reactions as way to resolve questions

B (p,Λ, Δ...), M (π, K , I...)

$$\bar{p} + p \rightarrow \bar{B}B + \bar{M}M$$

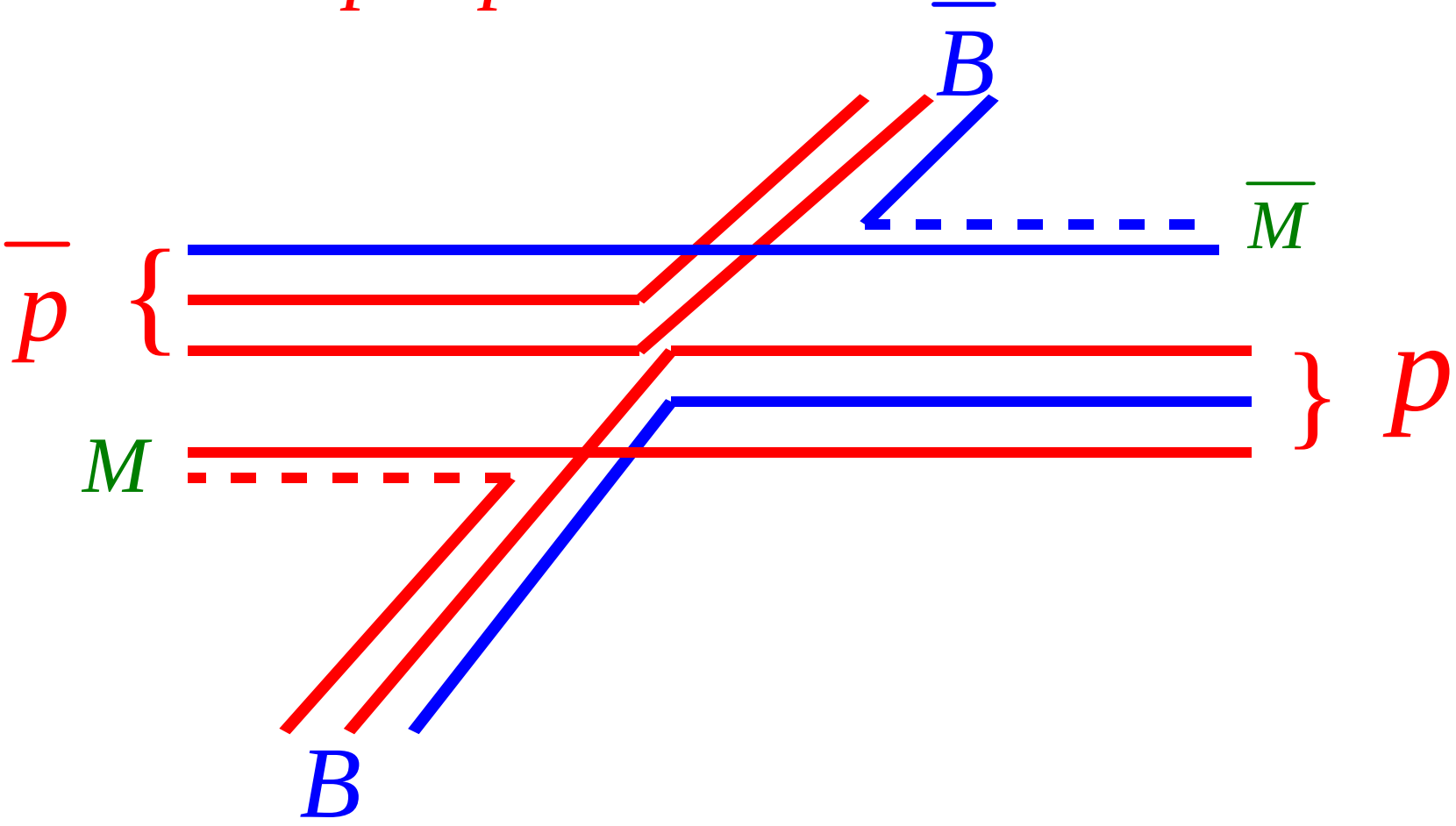

$\bar{p}p$ studies at $x_T \sim 1$

$$\left.\begin{array}{l} \bar{p}p \to \bar{p}p \\ \bar{p}p \to \bar{n}n - ? \end{array}\right\}$$

The counting rules and isotopic symmetry studies, $p_T \sim 2$ GeV/c anomaly(?)

$$\left.\begin{array}{l} \bar{p}p \to \bar{p}p + \pi\pi(KK) \\ \bar{p}p \to \bar{\Lambda}\Lambda + KK(\pi\pi, \mu\mu) \\ \bar{p}p \to \bar{\Delta}\Delta \end{array}\right\}$$

Detail vertexes studies:

$q(\bar{q}) + \bar{q}(q) - (quark - antiquark)$

$q(\bar{q}) + \bar{q}\bar{q}(qq) - (quark - antidiquark)$

$qq + \bar{q}\bar{q} - (diquark - antidiquark)$

Few words about nuclear target

$\overline{pA}$ reactions - Deep Inelastic Nuclear Reactions (DINR) at $x_T \sim 1$

DINR at high p_T as probes of the cold dense nuclear matter ($x_T > 1$)

Knot out cold dense nuclear configurations

SRC configuration

Multiquark configuration

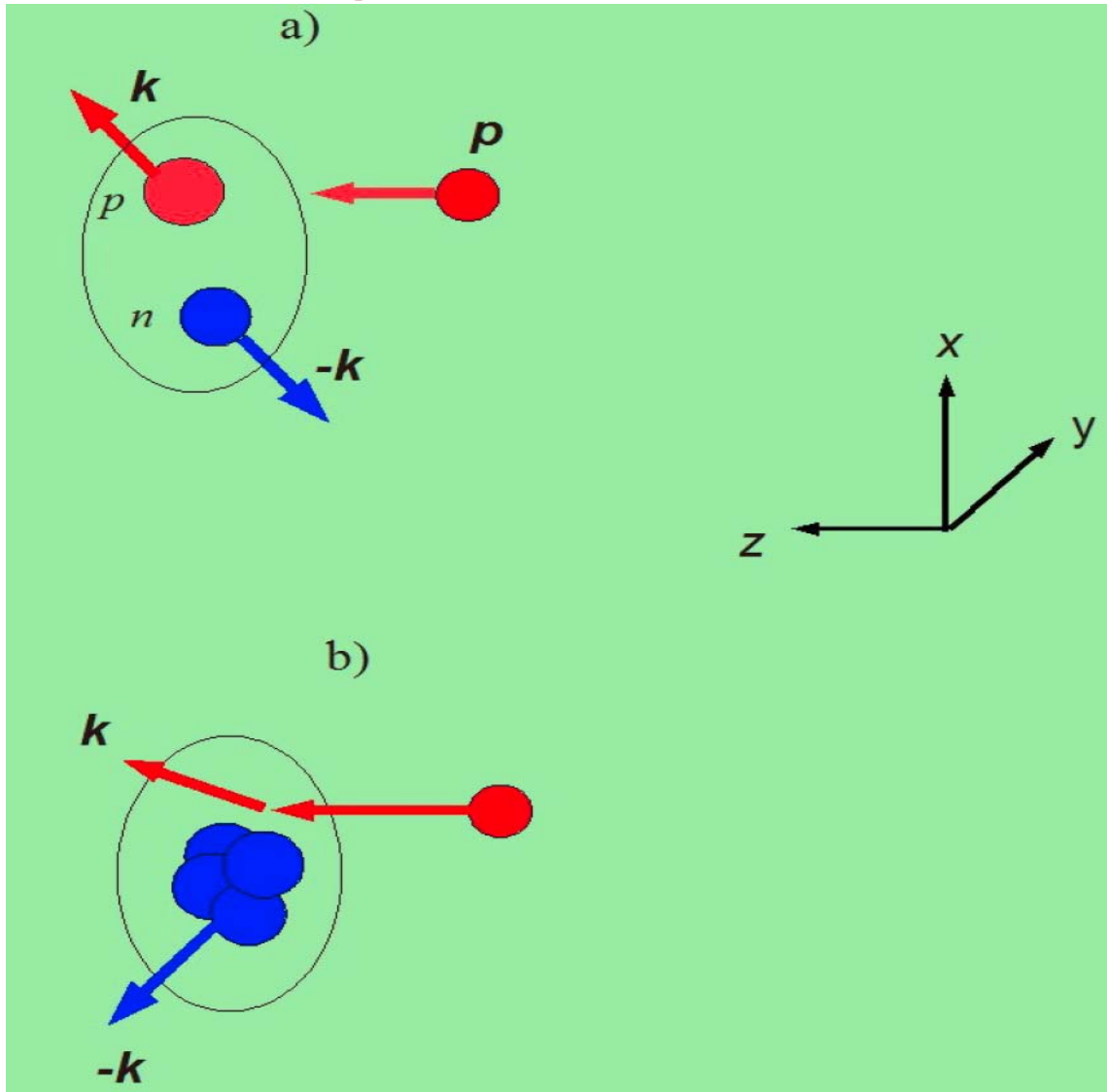

+

Subthreshold J/Ψ production.

The main questions for DINR at PANDA

1. Do we see multiquark states inside nuclei or it's SRC of nucleons?

2. Which properties of these objects?

CT (x_T = 1) with antiprotons

Color(nuclear) transparency in 90^0 c.m. quasielastic $A(p,2p)$ reactions

The incident momenta varied from 5.9 to 14.4 GeV/c, corresponding to $4.8 < Q^2 < 12.7$ (GeV/c)^2.

$$T = \frac{\frac{d\sigma}{dt}(p + \text{"}p\text{"} \rightarrow p + p)}{Z\frac{d\sigma}{dt}(p + p \rightarrow p + p)}$$

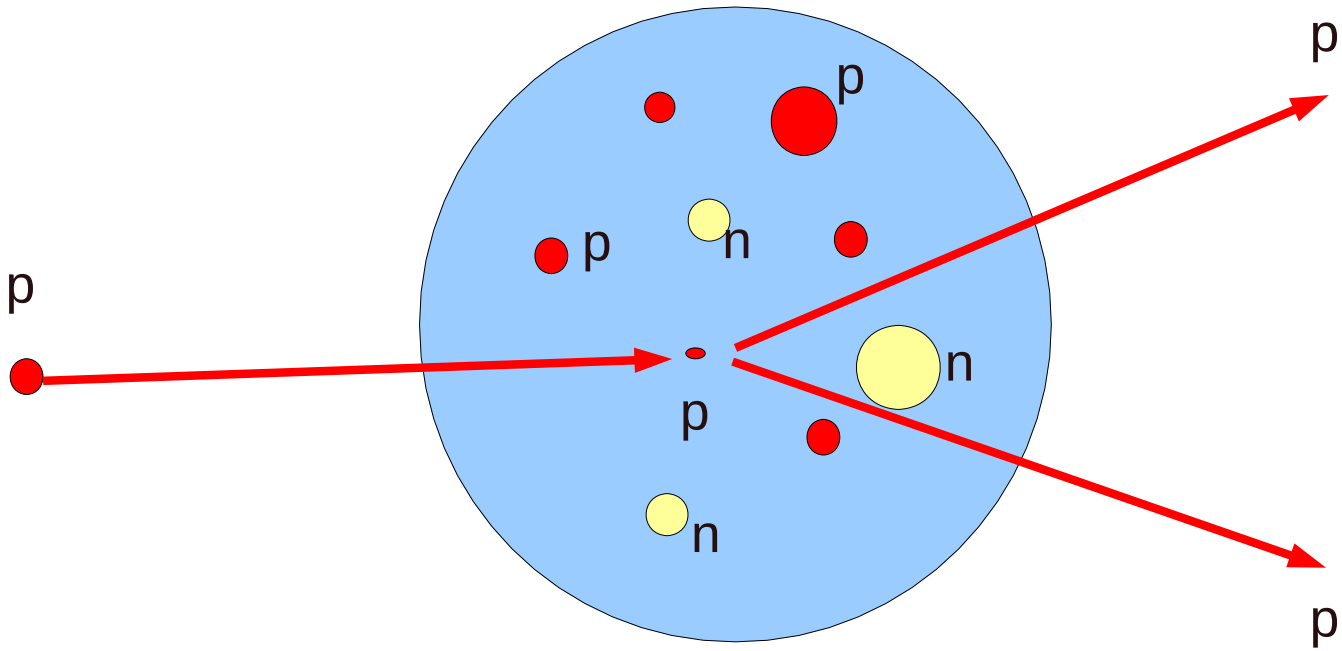

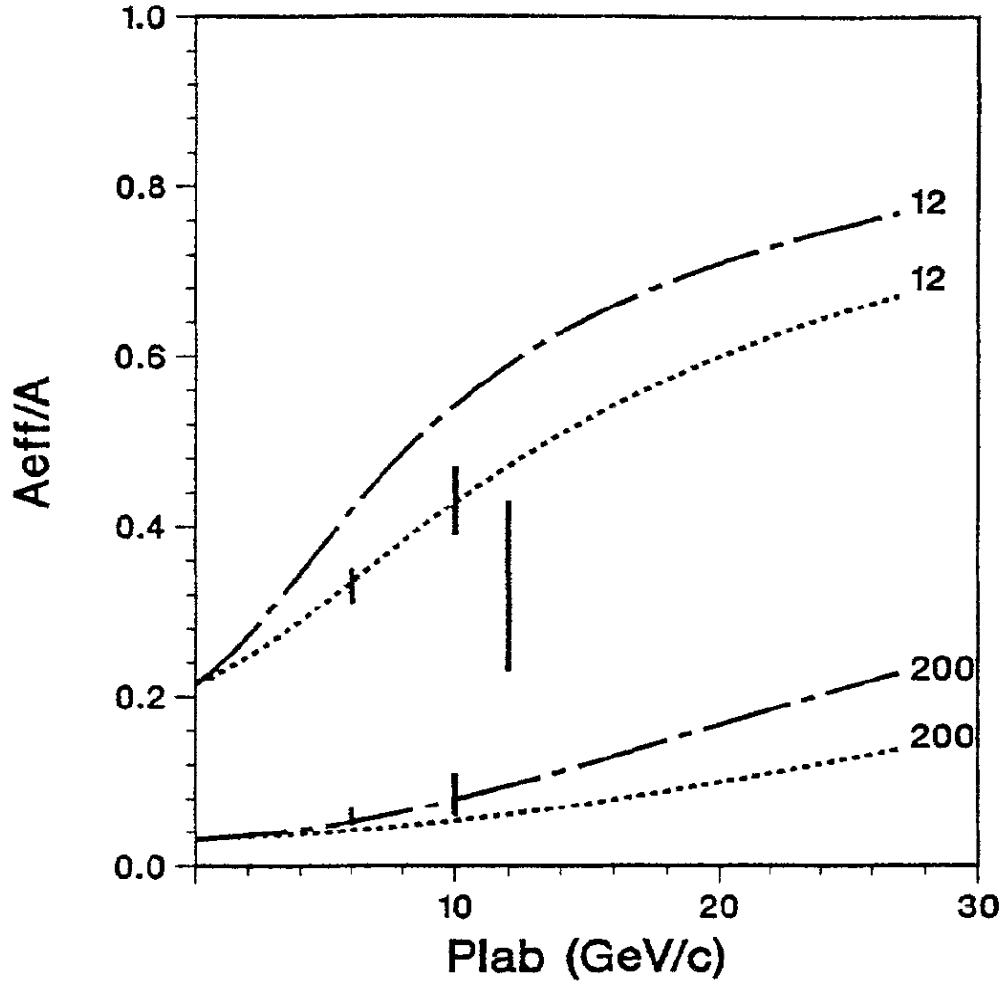

Fig. 3.8. The theoretical predictions of Farrar et al. [51] for $pA \to p'p''(A-1)$. The model predicts a monotonically increasing transparency ratio which is in clear conflict with the data, especially for the Al target (not shown; see Fig. 3.3).

nucl-th/0608040 v2 21 Nov 2006

A relativistic framework to determine the nuclear transparency from $A(p, 2p)$ reactions

B. Van Overmeire, J. Ryckebusch

Department of Subatomic and Radiation Physics, Ghent University, Proeftuinstraat 86, B-9000 Gent, Belgium

Abstract

A relativistic framework for computing the nuclear transparency extracted from $A(p, 2p)$ scattering processes is presented. The model accounts for the initial- and final-state interactions (IFSI) within the relativistic multiple-scattering Glauber approximation (RMSGA). For the description of color transparency, two existing models are used. The nuclear filtering mechanism is implemented as a possible explanation for the oscillatory energy dependence of the transparency. Results are presented for the target nuclei ^{7}Li, ^{12}C, ^{27}Al, and ^{63}Cu. An approximated, computationally less intensive version of the RMSGA framework is found to be sufficiently accurate for the calculation of the nuclear transparency. After including the nuclear filtering and color transparency mechanisms, our calculations are in acceptable agreement with the data.

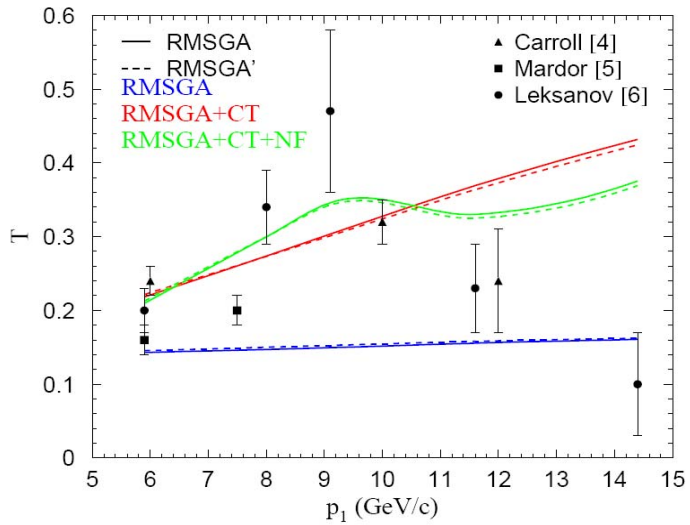

Fig. 1. The nuclear transparency for the ^{12}C$(p, 2p)$ reaction as a function the incoming lab momentum p_1. The full RMSGA (solid lines) are compared the RMSGA′ (dashed lines) results. The different curves represent the RMSG RMSGA+CT and RMSGA+CT+NF calculations. The CT effects are calculat in the FLFS model [21] with $\Delta M^2 = 0.7$ (GeV/c^2)^2 and the results including t mechanism of NF are obtained using the positive sign of $\phi(s) + \delta_1$. Data are fro Refs. [4,5,6].

Energy Dependence of Nuclear Transparency in C(p,2p) Scattering

A. Leksanov,[5] J. Alster,[1] G. Asryan,[3,2] Y. Averichev,[8] D. Barton,[3] V. Baturin,[5,4] N. Bukhtoyarova,[3,4] A. Carroll,[3] S. Heppelmann,[5] T. Kawabata,[6] Y. Makdisi,[3] A. Malki,[1] E. Minina,[5] I. Navon,[1] H. Nicholson,[7] A. Ogawa,[5] Yu. Panebratsev,[8] E. Piasetzky,[1] A. Schetkovsky,[5,4] S. Shimanskiy,[8] A. Tang,[9] J. W. Watson,[9] H. Yoshida,[6] and D. Zhalov[5]

[1]*School of Physics and Astronomy, Sackler Faculty of Exact Sciences, Tel Aviv University, Ramat Aviv 69978, Isra*
[2]*Yerevan Physics Institute, Yerevan 375036, Armenia*
[3]*Collider-Accelerator Department, Brookhaven National Laboratory, Upton, New York, 11973*
[4]*Petersburg Nuclear Physics Institute, Gatchina, St. Petersburg 188350, Russia*
[5]*Physics Department, Pennsylvania State University, University Park, Pennsylvania 16801*
[6]*Department of Physics, Kyoto University, Sakyoku, Kyoto, 606-8502, Japan*
[7]*Department of Physics, Mount Holyoke College, South Hadley, Massachusetts 01075*
[8]*J.I.N.R., Dubna, Moscow 141980, Russia*
[9]*Department of Physics, Kent State University, Kent, Ohio 44242*
(Received 20 April 2001; published 6 November 2001)

The transparency of carbon for $(p, 2p)$ quasielastic events was measured at beam momenta ranging from 5.9 to 14.5 GeV/c at 90° c.m. The four-momentum transfer squared (Q^2) ranged from 4.7 to 12.7 (GeV/c)^2. We present the observed beam momentum dependence of the ratio of the carbon to hydrogen cross sections. We also apply a model for the nuclear momentum distribution of carbon to obtain the nuclear transparency. We find a sharp rise in transparency as the beam momentum is increased to 9 GeV/c and a reduction to approximately the Glauber level at higher energies.

$$T_{\mathrm{CH}} = T \int d\alpha \int d^2\vec{P}_{FT}\, n(\alpha, \vec{P}_{FT}) \frac{(\frac{d\sigma}{dt})_{pp}(s(\alpha))}{(\frac{d\sigma}{dt})_{pp}(s_0)}$$

$$\alpha \equiv A \frac{(E_F - P_{Fz})}{M_A} \simeq 1 - \frac{P_{Fz}}{m_p}$$

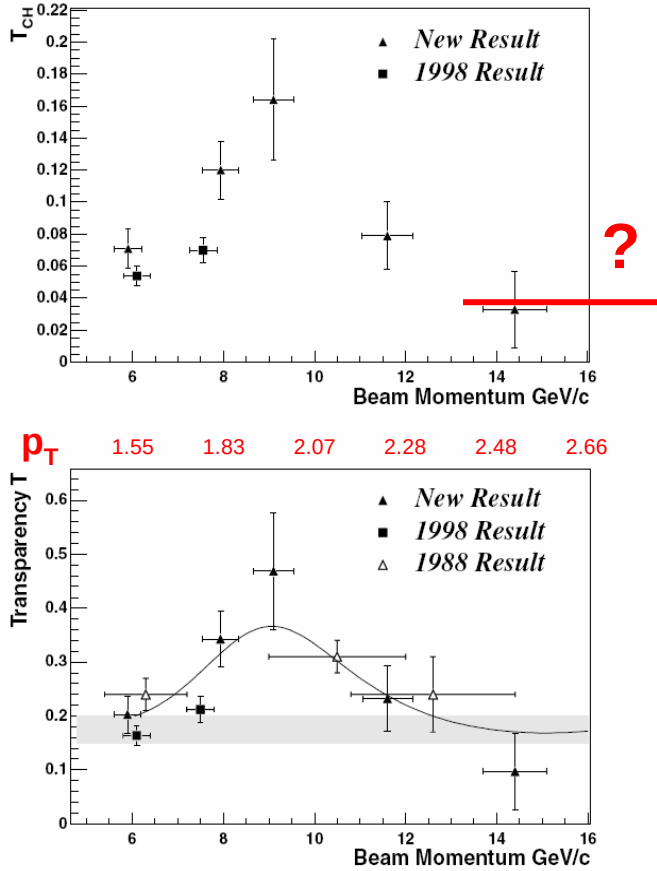

FIG. 2. Top: The transparency ratio T_{CH} as a function of the beam momentum for both the present result and two points from the 1998 publication [3]. Bottom: The transparency T versus beam momentum. The vertical errors shown here are all statistical errors, which dominate for these measurements. The horizontal errors reflect the α bin used. The shaded band represents the Glauber calculation for carbon [9]. The solid curve shows the shape R^{-1} as defined in the text. The 1998 data cover the c.m. angular region from 86°–90°. For the new data, a similar angular region is covered as is discussed in the text. The 1988 data cover 81°–90° c.m.

high p_t suppression seen by all experiments

R_{AA}=yield(AuAu)/N_{coll} yield(pp)

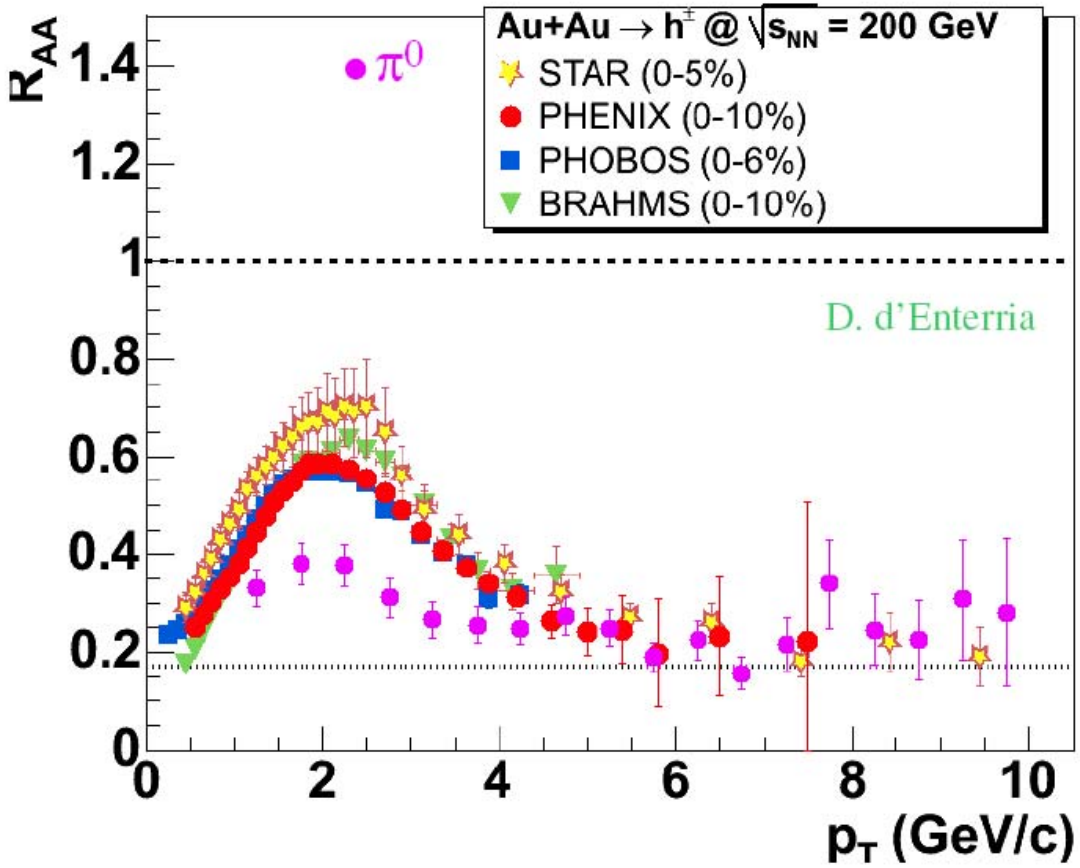

- all expts. see large suppression in AuAu
- π^0 lower than $h^{\pm}$
- no suppression in dAu rather Cronin enhancement → medium effect, not incoming partons

→ reasonable agreement between 4 experiments

QCD with and in nuclei: color transparency and short-range correlations in nuclei - theory, observations, directions for further studies

Mark Strikman
104 Davey Lab, Penn State University, University Park, PA 16802, USA

PANDA meeting, March 2009

Abstract

We summarize basic theoretical ideas which let to the observation of the short-range correlations (SRC) in nuclei using hard probes and outline directions for probing quark-gluon structure of SRCs. Implications of the observations of color transparency for processes involving pions are reviewed. Open questions and directions for further studies of color transparency phenomena using hadronic projectiles are presented using as an example the PANDA detector at FAIR.

Key words: short-range correlations, color transparency
PACS: 25.30.-c, 25.40.-h, 24.85.+p

Farrar has expressed meson-baryon scattering amplitudes as a sum of terms involving valence quark scattering amplitudes [17]. The amplitudes can be subdivided into four basic categories, shown in Fig. 1, which are described by pure gluon exchange (GEX), quark interchange (INT) between the hadrons, quark-antiquark annihilation (ANN) and pair creation, or a combination (COMB) of the above. The quark scattering amplitudes

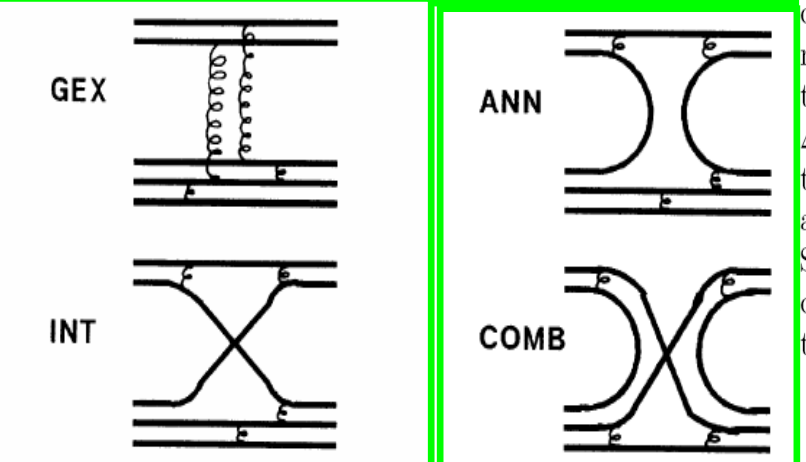

i. Study of the two body processes large angle processes with nucleon targets

Understanding of the large angle exclusive processes: $a + b \to c + d$ remains one of the challenges for pQCD. Systematic study of a large variety of reactions is available only for incident momentum of 6 and 9.9 GeV/c and below [27]. Analysis [27] found that cross sections of the processes where quark exchanges are allowed are much larger, and the energy dependence is roughly consistent with quark counting rules. Among the biggest puzzles is the ratio of $\theta_{c.m.} = 90^o$ cross sections of $\bar{p}p$ and pp elastic scattering which is below 4% at 6 GeV/c. At face value, it indicates extremely strong suppression of the diagrams with gluon exchanges in t channel, though more systematic, more precise studies are clearly necessary. Another puzzle is the oscillation of the differential cross section of the elastic pp scattering at large t around a smooth quark counting inspired parametrization. Are these oscillations present in any of the $p\bar{p}$ channels?

It appears that PANDA will have excellent acceptance for numerous large angle processes - from the simplest processes $p\bar{p} \to p\bar{p}, \pi\pi, K\bar{K}$ to the processes of production of multi particle states: baryon - antibaryon and meson pairs, etc. In the case of the proton beam the elastic channel is covered reasonably well, though the channels involving Δ-isobars, nonresonance πN production, etc are practically not known. Another gap in the knowledge is pn scattering which could be studied using the ^{2}H pellets. There is a suggestion that the measurement of the pn/pp ratio may provide an insight on the SU(6) structure of the nucleon wave function at large x [28]. Overall, comparing all these channels in pN and $\bar{p}N$ scattering may lead to a break through in understanding hard two body reactions.

END

$$\frac{d\sigma}{d\Omega} = \frac{\text{events}}{I_0 \Delta\Omega N_0 \rho t}.$$

Here I_0 is the incident proton beam flux as measured by Be^{7*} decays, and $\Delta\Omega$ is the center-of-mass solid angle which was around 2×10^{-4} sr. The quantity N_0 is Avogadro's number taken to be $6.02\ 10^{23}$; t is the target thickness, either 1 or 2 cm; and ρ is the density of hydrogen protons in our block of CH_2 which was measured to be 0.131 moles/cm³. The number of events was corrected as discussed above.

Finally, this experiment eliminated confusion about the choice of the correct variable. Since all cross sections were measured at 90^0 where $\sin\theta=1$ and $\cos\theta=0$; we have that $P_{c.m.}^2=P_1^2=-t/2$. Thus, both variables were proportional to each other and there was no confusion.

TABLE I. Proton-proton elastic scattering cross sections at 90° in the center-of-mass system.

$P_{c.m.}^2$ (GeV/c)²	P_0 (GeV/c)	$(d\sigma/d\Omega)_{c.m.}$ (μb/sr)	$(d\sigma/dt)_{c.m.}$ μb/(GeV/c)²	Error in $d\sigma/d\Omega$ & $d\sigma/d$ %
1.946	5.0	8.51	13.74	2.9
1.993	5.1	7.90	12.45	3.3
2.039	5.2	7.09	10.93	3.1
2.086	5.3	6.49	9.77	3.6
2.132	5.4	5.53	8.15	3.1
2.178	5.5	4.90	7.07	3.4
2.223	5.6	4.47	6.32	3.1
2.270	5.7	3.72	5.15	3.3
2.316	5.8	3.37	4.57	3.3
2.363	5.9	2.74	3.64	3.5
2.409	6.0	2.44	3.18	3.1
2.456	6.1	2.19	2.80	3.7
2.503	6.2	1.83	2.30	3.7
2.595	6.4	1.50	1.82	3.7
2.686	6.6	1.07	1.25	4.7
2.779	6.8	0.796	0.900	4.7
2.873	7.0	0.645	0.706	4.1
2.965	7.2	0.515	0.546	4.0
3.059	7.4	0.386	0.396	4.8
3.151	7.6	0.305	0.304	5.4
3.247	7.8	0.253	0.245	4.5
3.338	8.0	0.217	0.204	4.5
3.386	8.1	0.169	0.157	3.9
3.434	8.2	0.172	0.157	4.4
3.480	8.3	0.154	0.139	3.8
3.527	8.4	0.153	0.136	4.6
3.618	8.6	0.127	0.110	4.6
3.713	8.8	0.103	0.0871	4.8
3.806	9.0	0.0809	0.0667	4.6
3.897	9.2	0.0780	0.0629	4.3
3.992	9.4	0.0676	0.0532	5.3
4.084	9.6	0.0589	0.0453	4.9
4.178	9.8	0.0536	0.0403	4.7
4.272	10.0	0.0468	0.0344	4.9
4.364	10.2	0.0441	0.0318	4.8
4.461	10.4	0.0386	0.0272	4.7
4.554	10.6	0.0356	0.0246	4.8
4.644	10.8	0.0303	0.0205	4.9
4.739	11.0	0.0284	0.0188	5.5
4.831	11.2	0.0255	0.0166	5.4
4.924	11.4	0.0202	0.0129	5.4
5.018	11.6	0.0190	0.0119	5.2
5.112	11.8	0.0153	0.00940	5.4
5.208	12.0	0.0143	0.00862	5.4
5.299	12.2	0.0118	0.00699	5.3
5.392	12.4	0.0116	0.00676	5.4
5.490	12.6	0.00953	0.00545	6.3
5.579	12.8	0.00867	0.00488	5.7
5.674	13.0	0.00739	0.00409	5.9
5.770	13.2	0.00722	0.00393	7.1
5.861	13.4	0.00525	0.00281	5.7

Elastic Proton-Proton Scattering at 90° and Structure within the Proton*

C. W. AKERLOF, R. H. HIEBER, A. D. KRISCH
Randall Laboratory of Physics, University of Michigan, Ann Arbor, Michigan

AND

K. W. EDWARDS†
Department of Physics, University of Iowa, Iowa City, Iowa

AND

L. G. RATNER
Particle Accelerator Division, Argonne National Laboratory, Argonne, Illinois

AND

K. RUDDICK‡
Department of Physics, University of Minnesota, Minneapolis, Minnesota

(Received 3 January 1964)

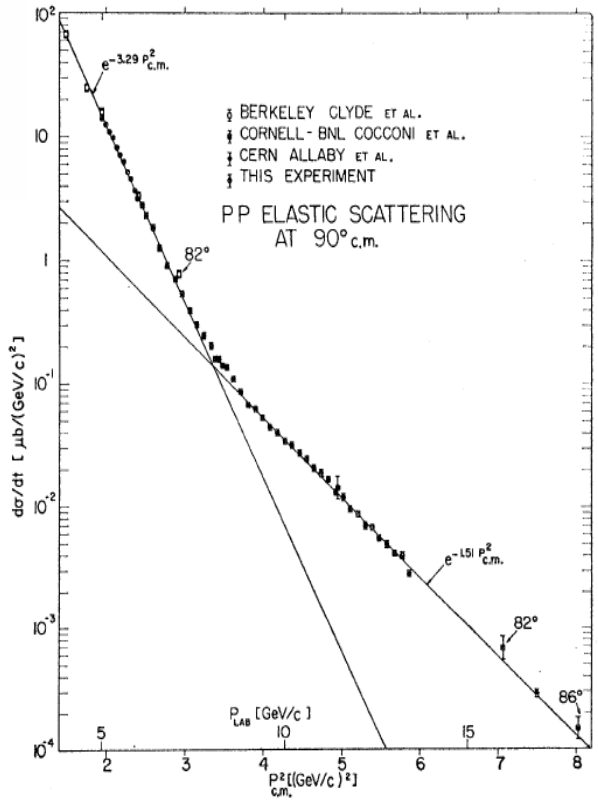

FIG. 8. Plot of $d\sigma/d\Omega$ versus $P_{\text{c.m.}}$ for 90° proton-proton elastic scattering. Other data (Refs. 20, 22, 23) are also plotted. The line drawn is the straight line fit suggested by the statistical model.

p.296-300

PRECISION MEASUREMENTS OF THE ANTIPROTON–PROTON ELASTIC SCATTERING CROSS SECTION AT 90° IN THE INCIDENT MOMENTUM RANGE BETWEEN 3.5 GeV/c AND 5.7 GeV/c

R-704 Collaboration

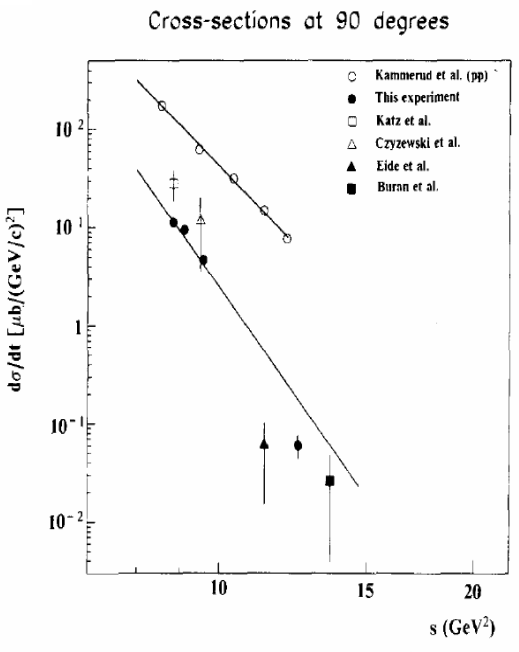

Fig. 3. The $p\bar{p}$ and pp elastic differential cross sections at 90° CM as function of the square of the CM energy, s. Open circles are pp data from ref. [6]. These data fit well to the drawn curve proportional to s^{-9}. The remaining points are $p\bar{p}$ data. Shaded from this experiment. Otherwise from ref. [7] (open square), ref. [8] (open triangle) ref. [9] (shaded triangle) and ref. [10] (shaded square). The lower curve is an s^{-n} fit to four data points of this experiment, neglecting systematic errors. One obtains $n = 12.3 \pm 0.2$, but evidently the data do not seem to follow this kind of a power law.

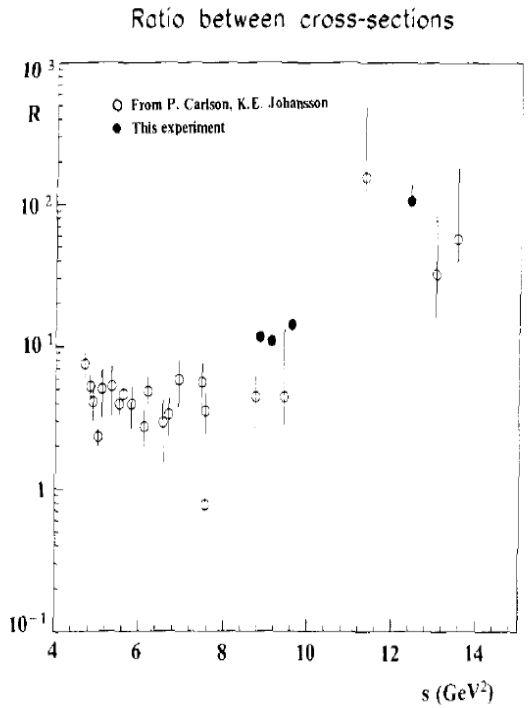

Fig. 4. The ratio between pp and $p\bar{p}$ elastic cross sections at 90° as function of s. The figure is taken from ref. [13] with our data points (shaded circles) added. The pp data used for calculating these ratios for our data points are from ref. [6].

conditions. The cross section is given by

$$\frac{d\sigma}{d\Omega} = \frac{N - N_B}{2\pi\Delta\cos(\theta^*)LK}, \qquad (1)$$

where N is the number of events, N_B is the number of background events, $\Delta\cos(\theta^*)$ is the range in the cosine of the scattering angle at which events were collected ($\Delta\cos(\theta^*)=0.08$), L is the integrated luminosity and K is a correction factor accounting for geometrical acceptance and inefficiencies. The geometrical acceptance was calculated by Monte Carlo and found to be ranging between 21% and 25%, depending on incident momentum and trigger matrix setting. The correction factor due to the tight trigger

Table 1
Summary of results for the measurements of the antiproton–proton elastic scattering cross section at 90° CM.

P [GeV/c]	N	L [nb^{-1}]	$d\sigma/d\Omega$ [μb/ster]	$-t$ [(GeV/c)^2]	$d\sigma/dt$ [μb/(GeV/c)^2]	Relative error (%)	
						stat	syst
3.65	3151	12.04	4.75	2.65	11.20	1.8	10.0
3.83	684	2.16	4.12	2.78	9.29	3.8	10.0
4.07	1577	10.32	2.23	3.03	4.61	2.6	10.0
5.65	107	21.06	0.043	4.50	0.060	19.0	13.0